

# Discretized Fast-Slow Systems with Canard Points in Two Dimensions

Maximilian Engel\*, Christian Kuehn\*, Matteo Petrera† and Yuri Suris†

16th July 2019

## Abstract

We study the behaviour of slow manifolds for two different discretization schemes of fast-slow systems with canard fold points. The analysis uses the blow-up method to deal with the loss of normal hyperbolicity at the canard point. While the Euler method does not preserve the folded canard, we can show that the Kahan discretization allows for a similar result as in continuous time, guaranteeing the occurrence of canard connections between attracting and repelling slow manifolds upon variation of a bifurcation parameter. Furthermore, we investigate the existence and properties of a formal conserved quantity in the rescaled Kahan map.

**Keywords:** slow manifolds, invariant manifolds, blow-up method, loss of normal hyperbolicity, discretization, maps, canards.

**Mathematics Subject Classification (2010):** 34E15, 34E20, 37M99, 37G10, 34C45, 39A99.

## 1 Introduction

Systems with canards through fold points can be studied starting from the ordinary differential equation (ODE)

$$\begin{aligned}x' &= -y + x^2, \\y' &= \varepsilon(x - \lambda),\end{aligned}\tag{1.1}$$

where we interpret  $\varepsilon > 0$  as a small time scale separation parameter between the fast variable  $x$  and the slow variable  $y$ . System (1.1) represents the simplest normal form of a fast-slow system exhibiting a *canard point* at the origin for  $\lambda = 0$ . The canard point is a fold point past whom trajectories connect an attracting slow manifold and a repelling slow manifold, also described as *canard solution* [1, 6, 17]. The origin is called singular since hyperbolicity of the dynamics breaks down at this point.

When the vector field in equation (1.1) contains additional perturbation terms in  $x, y, \varepsilon, \lambda$ , a functional relation between  $\lambda$  and  $\varepsilon$  can be discovered that guarantees the existence of such canards beyond the form (1.1) with  $\lambda = 0$ .

---

\*TU Munich

†TU Berlin

Krupa and Szmolyan [15] have analyzed canard extensions for perturbations of equation (1.1) by using the *blow-up method* which allows to deal with the nonhyperbolic singularity at the origin. The key idea to use the blow-up method [4, 5] for fast-slow systems goes back to Dumortier and Roussarie [6]. They observed that this technique may convert non-hyperbolic singularities at which fast and slow directions interact into partially hyperbolic problems. The method inserts a suitable manifold, e.g. a sphere, at the singularity and describes the extension of hyperbolic objects through a neighbourhood of the singularity via the partially hyperbolic dynamics on this manifold; see e.g. [19, Chapter 7] for an introduction and [23, 22, 24, 10, 15, 18, 20] for a list of a few, yet by no means exhaustive, list of different applications to planar fast-slow systems. The dynamics on the manifold are usually analyzed in different charts.

The crucial observation for proving the extension of canards in [15] is the existence of a constant of motion for the dynamics in the *rescaling chart*  $K_2$  in the blown-up space. This constant of motion can be used for a *Melnikov method* which computes the separation of the attracting and repelling manifold under perturbations, in particular giving the parameter combinations of  $\varepsilon$  and  $\lambda$  for which the manifolds still intersect such that a canard connection is formed.

The observation of this constant of motion suggests that the time discretization of the canard problem demands for a structure preserving method in order to retain the property of canard connections. We investigate time discretization of the ODE (1.1) via the Kahan-Hirota-Kimura discretization scheme (see e.g. [14, 26]) that has produced *integrable* maps, i.e. maps that conserve a certain quantity, in several examples of quadratic vector fields. Introducing the step size  $h > 0$ , the Kahan discretization of the ODE (1.1) gives the two-dimensional map

$$P_K : \begin{pmatrix} x \\ y \end{pmatrix} \rightarrow \begin{pmatrix} \tilde{x} \\ \tilde{y} \end{pmatrix} = \begin{pmatrix} \frac{x - hy - \frac{h^2}{4}\varepsilon x + \frac{h^2}{2}\lambda\varepsilon}{1 - hx + \frac{h^2}{4}\varepsilon} \\ \frac{y - h y x - \frac{h^2}{2}\varepsilon x^2 - h\lambda\varepsilon + h^2 x \lambda \varepsilon + h\varepsilon x - \frac{h^2}{4}\varepsilon y}{1 - hx + \frac{h^2}{4}\varepsilon} \end{pmatrix}. \quad (1.2)$$

In particular, we will compare the properties of this scheme with the explicit Euler discretization of equation (1.1), given by

$$P_E : \begin{pmatrix} x \\ y \end{pmatrix} \rightarrow \begin{pmatrix} \tilde{x} \\ \tilde{y} \end{pmatrix} = \begin{pmatrix} x + h(x^2 - y) \\ y + \varepsilon h(x - \lambda) \end{pmatrix}. \quad (1.3)$$

The loss of hyperbolicity at the origin also holds for the maps (1.2) and (1.3). This suggests to apply the blow-up method, which has so far mainly been used for flows, to the fast-slow dynamical systems induced by these two maps. In that way we add the problem of folded canard solutions to the list of key examples for discrete-time fast slow systems with non-hyperbolic singularities that can be compared to continuous-time analogues, as already seen in the cases of the fold singularity [25], the transcritical singularity [7] and the pitchfork singularity [21]. In the latter two cases also canards turned up that could easily be preserved by the Euler schemes.

In the situation of the folded canard problem, the integrable structure turns out to be crucial also for choosing the appropriate discretization scheme. In this paper we show that the Kahan map (1.2) exhibits canards for  $\lambda = 0$ , while the Euler map (1.3), for  $h > 0$  fixed and sufficiently small fixed  $\varepsilon > 0$ , does not. In particular, we find that, in the rescaling chart  $K_2$  of the blow-up, the Kahan discretization has an invariant curve with special trajectory  $\gamma_h$ , separating bounded and unbounded solutions, analogously to the ODE case. Such a curve is shown not to exist for the Euler discretization.

Adding (quadratic) perturbations in  $x, y, \varepsilon, \lambda$  to the normal form (1.1), the corresponding Kahan discretization can further be shown to provide canard extensions for a functional relation between  $\lambda$  and  $\varepsilon$ , coinciding with the ODE result [15] up to leading order. The proof uses a discrete-time Melnikov method making use of the separatrix solution  $\gamma_h$  in the rescaling chart  $K_2$ . The re-transition to the original coordinates also depends on a detailed analysis of the entering and exiting chart  $K_1$  where the attracting and repelling manifolds and their transition into  $K_2$  are established.

The remainder of the paper is structured as follows. Section 2 recalls the setting of fast-slow systems in continuous time and summarizes the main result on folded canard extensions, Theorem 2.1, with a short sketch of the proof, as given in [15]. In Section 3, we turn to the problem of corresponding discretization schemes, establishing the blow-up transformation for the discretized problem in Section 3.1. We discuss the Euler discretization and its failure to preserve the canard structure in Section 3.2. The remainder of Section 3 then discusses the various results and insights for the Kahan scheme: while in Section 3.3.1 the dynamics in the entering and exiting chart  $K_1$  are analyzed, the existence of the separatrix solution in the rescaling chart  $K_2$  and its transitions into  $K_1$  are established in Section 3.3.2, where we also discuss the role of a formal conserved quantity. After briefly treating a potential symplectic discretization of the rescaled ODE system transformed into Hamiltonian coordinates, we conduct the Melnikov computation along the invariant curve in Section 3.3.4, leading to the proof of Theorem 3.10, which is the discrete-time analogue to Theorem 2.1.

**Acknowledgements:** The authors gratefully acknowledge support by the DFG via the SFB/TR109 Discretization in Geometry and Dynamics. CK acknowledges support by a Lichtenberg Professorship of the VolkswagenFoundation.

## 2 Canard extension through a fold in continuous time

### 2.1 Fast-slow systems

We start with a brief review and notation for continuous-time fast-slow systems. Consider a system of singularly perturbed ordinary differential equations (ODEs) of the form

$$\begin{aligned} \varepsilon \frac{dx}{d\tau} &= \varepsilon \dot{x} = f(x, y, \varepsilon), \\ \frac{dy}{d\tau} &= \dot{y} = g(x, y, \varepsilon), \quad x \in \mathbb{R}^m, \quad y \in \mathbb{R}^n, \quad 0 < \varepsilon \ll 1, \end{aligned} \tag{2.1}$$

where  $f, g$ , are  $C^k$ -functions with  $k \geq 3$ . Since  $\varepsilon$  is a small parameter, the variables  $x$  and  $y$  are often called the *fast* variable(s) and the *slow* variable(s) respectively. The time variable in (2.1), denoted by  $\tau$ , is termed the *slow* time scale. The change of variables to the *fast* time scale  $t := \tau/\varepsilon$  transforms the system (2.1) into the ODEs

$$\begin{aligned} x' &= f(x, y, \varepsilon), \\ y' &= \varepsilon g(x, y, \varepsilon). \end{aligned} \tag{2.2}$$

Both equations correspond with a respective limiting problem for  $\varepsilon = 0$ : the *reduced problem* (or *slow subsystem*) is given by

$$\begin{aligned} 0 &= f(x, y, 0), \\ \dot{y} &= g(x, y, 0), \end{aligned} \tag{2.3}$$

and the *layer problem* (or *fast subsystem*) is

$$\begin{aligned}x' &= f(x, y, 0), \\y' &= 0.\end{aligned}\tag{2.4}$$

We can understand the reduced problem (2.3) as a dynamical system on the *critical manifold*

$$S_0 = \{(x, y) \in \mathbb{R}^{m+n} : f(x, y, 0) = 0\}.$$

Observe that the manifold  $S_0$  consists of equilibria of the layer problem (2.4).  $S_0$  is called *normally hyperbolic* if the matrix  $D_x f(p) \in \mathbb{R}^{m \times m}$  for all  $p \in S_0$  has no spectrum on the imaginary axis. For a normally hyperbolic  $S_0$  *Fenichel Theory* [8, 13, 19, 29] implies that for  $\varepsilon$  sufficiently small, there is a locally invariant slow manifold  $S_\varepsilon$  such that the restriction of (2.1) to  $S_\varepsilon$  is a regular perturbation of the reduced problem (2.3). Furthermore, it follows from Fenichel's perturbation results that  $S_\varepsilon$  possesses an invariant stable and unstable foliation, where the dynamics behave as a small perturbation of the layer problem (2.4).

A challenging phenomenon is the breakdown of normal hyperbolicity of  $S_0$  such that Fenichel Theory cannot be applied. Typical examples of such a breakdown are found at bifurcation points  $p \in S_0$ , where the Jacobian  $D_x f(p)$  has at least one eigenvalue with zero real part. The simplest examples are folds or points of transversal self-intersection of  $S$  in planar systems ( $m = 1 = n$ ). In the following we focus on the particularly challenging problem of fold points admitting (maximal) *canard solutions*.

## 2.2 Main result on folded canard extension

We introduce an additional real parameter  $\lambda$  and consider a family of planar ODEs similar to (2.2), namely,

$$\begin{aligned}x' &= f(x, y, \lambda, \varepsilon), \\y' &= \varepsilon g(x, y, \lambda, \varepsilon).\end{aligned}\tag{2.5}$$

We assume that at  $\lambda = \varepsilon = 0$ , the vector fields  $f$  and  $g$  satisfy the conditions of a *folded singularity* at  $(x_0, y_0) = (0, 0)$  as well as of a *canard point* (see [15] for details). By a local change of coordinates, the canard point problem can be brought into the canonical form

$$\begin{aligned}x' &= -yk_1(x, y, \lambda, \varepsilon) + x^2k_2(x, y, \lambda, \varepsilon) + \varepsilon k_3(x, y, \lambda, \varepsilon), \\y' &= \varepsilon(xk_4(x, y, \lambda, \varepsilon) - \lambda k_5(x, y, \lambda, \varepsilon) + yk_6(x, y, \lambda, \varepsilon)),\end{aligned}\tag{2.6}$$

where

$$\begin{aligned}k_i(x, y, \lambda, \varepsilon) &= \mathcal{O}(x, y, \lambda, \varepsilon), \quad i = 3, 6, \\k_j(x, y, \lambda, \varepsilon) &= 1 + \mathcal{O}(x, y, \lambda, \varepsilon), \quad j = 1, 2, 4, 5.\end{aligned}\tag{2.7}$$

For  $\lambda = 0$  the critical manifold

$$S_0 := \{(x, y) \in \mathbb{R}^2 : f(x, y, 0, 0) = 0\}$$

is the union of two branches  $S_a$  and  $S_r$  where  $a$  means attracting and  $r$  repelling (see e.g. [19, Figure 8.1]). We denote the corresponding slow manifolds for small  $\varepsilon > 0$  by  $S_{a,\varepsilon}$  and  $S_{r,\varepsilon}$ .

Solving the equation  $f(x, y, 0, 0) = 0$  for  $y$  as a function of  $x$  with  $y = \varphi(x)$ , gives the reduced dynamics on  $S_0$

$$\dot{x} = \frac{g(x, \varphi(x), 0, 0)}{\varphi'(x)}. \quad (2.8)$$

In our setting, the function at the right-hand side is smooth at the origin such that the reduced flow goes through the origin via a maximal solution  $x_0(t)$  of (2.8) with  $x_0(0) = 0$ . In the easiest example  $k_i = 0$  for  $i = 3, 6$  and  $k_j = 1$  for  $j = 1, 2, 4, 5$ , we obtain  $2x\dot{x} = x$  and, hence,  $\dot{x} = 1/2$ , desingularized at  $x = 0$ . Thus, there is a solution  $x_0(t)$  which connects  $S_a$  and  $S_r$ , where  $S_a$  is the left and  $S_r$  the right branch of the parabola  $\{y = x^2\}$ . Krupa and Szmolyan show that for sufficiently small  $\varepsilon > 0$  there exists also a connection from  $S_{a,\varepsilon}$  to  $S_{r,\varepsilon}$  along a curve in the  $(\lambda, \varepsilon)$ -plane.

In more detail, for  $j = a, r$ , we define  $\Delta_j := \{(x, \rho^2), x \in I_j\}$  as sections of  $S_j$  with  $\rho > 0$  sufficiently small and intervals  $I_j$ . Furthermore, we set  $q_{j,\varepsilon} = \Delta_j \cap S_{j,\varepsilon}$  and let  $\pi$  be the transition map from  $\Delta_a$  to  $\Delta_r$  along the flow of (2.6). Introducing the quantities

$$\begin{aligned} a_1 &:= \frac{\partial k_3}{\partial x}(0, 0, 0, 0), & a_2 &:= \frac{\partial k_1}{\partial x}(0, 0, 0, 0), & a_3 &:= \frac{\partial k_2}{\partial x}(0, 0, 0, 0), \\ a_4 &:= \frac{\partial k_4}{\partial x}(0, 0, 0, 0), & a_5 &:= k_6(0, 0, 0, 0). \end{aligned} \quad (2.9)$$

we can write the main result on extensions of canard solutions, as given in [15, Theorem 3.1].

**Theorem 2.1.** *Consider system (2.6) such that the solution  $x_0(t)$  of the reduced problem connects  $S_a$  and  $S_r$ . Then there exist  $\varepsilon_0 > 0$  and a smooth function  $\lambda_c(\sqrt{\varepsilon})$  defined on  $[0, \varepsilon_0]$  such that for  $\varepsilon \in [0, \varepsilon_0]$  the following holds:*

1. *The attracting slow manifold  $S_{a,\varepsilon}$  and the repelling slow manifold  $S_{r,\varepsilon}$  intersect, i.e. exhibit a maximal canard such that  $\pi(q_{a,\varepsilon}) = q_{r,\varepsilon}$ , if and only if  $\lambda = \lambda_c(\sqrt{\varepsilon})$ .*
2. *The function  $\lambda_c$  has the expansion*

$$\lambda_c(\sqrt{\varepsilon}) = -C\varepsilon + \mathcal{O}(\varepsilon^{3/2}),$$

where the constant  $C$  is given by

$$C = \frac{1}{8} (4a_1 - a_2 + 3a_3 - 2a_4 + 2a_5). \quad (2.10)$$

3. *The map  $\pi$  is only defined for  $\lambda$  in an interval around  $\lambda_c(\sqrt{\varepsilon})$  of width  $\mathcal{O}(e^{-c/\varepsilon})$  for some  $c > 0$ .*

## 2.3 Role of a constant of motion for proving the canard result

In order to use specific geometric methods in singular perturbation theory, we consider  $\varepsilon$  and  $\lambda$  as variables, writing

$$\begin{aligned} x' &= -yk_1(x, y, \lambda, \varepsilon) + x^2k_2(x, y, \lambda, \varepsilon) + \varepsilon k_3(x, y, \lambda, \varepsilon), \\ y' &= \varepsilon(xk_4(x, y, \lambda, \varepsilon) - \lambda k_5(x, y, \lambda, \varepsilon) + yk_6(x, y, \lambda, \varepsilon)), \\ \varepsilon' &= 0, \\ \lambda' &= 0. \end{aligned} \quad (2.11)$$

Note that the Jacobian of the above vector field in  $(x, y, \lambda, \varepsilon)$  has a quadruple zero eigenvalue at the origin. A well established way to gain hyperbolicity at this singularity is the *blow-up technique* which identifies the singularity with a manifold on which the dynamics can be desingularized. An important ingredient of this technique is that the vector field  $f : \mathbb{R}^n \rightarrow \mathbb{R}^n$  of the ODE is *quasihomogeneous* (cf. [19, Definition 7.3.2]), which means that there are  $(a_1, \dots, a_n) \in \mathbb{N}^n$  and  $k \in \mathbb{N}$  such that for every  $r \in \mathbb{R}$  and each component  $f_j : \mathbb{R}^n \rightarrow \mathbb{R}$  of  $f$  we have

$$f_j(r^{a_1}z_1, \dots, r^{a_n}z_n) = r^{k+a_j} f_j(z_1, \dots, z_n).$$

We consider the sphere  $S^2 := \{(\bar{x}, \bar{y}, \bar{\varepsilon}) : \bar{x}^2 + \bar{y}^2 + \bar{\varepsilon}^2 = 1\}$ . The proof of Theorem 2.1 in [15] uses the (up to leading order) quasihomogeneous *blow-up transformation*

$$x = r\bar{x}, \quad y = r^2\bar{y}, \quad \varepsilon = r^2\bar{\varepsilon}, \quad \lambda = r\bar{\lambda},$$

where  $(\bar{x}, \bar{y}, \bar{\varepsilon}, \bar{\lambda}, r) \in B := S^2 \times [-\kappa, \kappa] \times [0, \rho]$  for some  $\kappa, \rho > 0$ . The transformation can be formalised as a map  $\Phi : B \rightarrow \mathbb{R}^4$ , where  $\rho$  and  $\kappa$  are small enough such that the dynamics on  $\Phi(B)$  can be described by the normal form approximation. The map  $\Phi$  induces a vector field  $\bar{X}$  on  $B$  by  $\Phi_*(\bar{X}) = X$ , where  $\Phi_*$  is the pushforward induced by  $\Phi$ . The associated dynamics on  $B$  are analyzed in two charts  $K_i, i = 1, 2$ , an entering and exiting chart  $K_1$  ( $\bar{y} = 1$ ) and a scaling chart  $K_2$  ( $\bar{\varepsilon} = 1$ ), given by

$$K_1 : \quad x = r_1x_1, \quad y = r_1^2, \quad \varepsilon = r_1^2\varepsilon_1, \quad \lambda = r_1\lambda_1, \quad (2.12)$$

$$K_2 : \quad x = r_2x_2, \quad y = r_2^2y_2, \quad \varepsilon = r_2^2, \quad \lambda = r_2\lambda_2. \quad (2.13)$$

The main point of interest are the dynamics in chart  $K_2$  where the transformed equations, after dividing out a factor  $r_2$ , have the form

$$\begin{aligned} x_2' &= -y_2 + x_2^2 + r_2G_1(x_2, y_2) + \mathcal{O}(r_2(\lambda_2 + r_2)), \\ y_2' &= x_2 - \lambda_2 + r_2G_2(x_2, y_2) + \mathcal{O}(r_2(\lambda_2 + r_2)), \\ r_2' &= 0, \\ \lambda_2' &= 0, \end{aligned} \quad (2.14)$$

where  $G = (G_1, G_2)$  can be written explicitly as

$$G(x, y) = \begin{pmatrix} G_1(x, y) \\ G_2(x, y) \end{pmatrix} = \begin{pmatrix} a_1x - a_2xy + a_3x^3 \\ a_4x^2 + a_5y \end{pmatrix}. \quad (2.15)$$

On the invariant set  $\{r_2 = 0 = \lambda_2\}$ , we have

$$\begin{aligned} x_2' &= -y_2 + x_2^2, \\ y_2' &= x_2. \end{aligned} \quad (2.16)$$

The crucial observation (cf. [15, Lemma 3.3]) is that system (2.16) is integrable with the constant of motion

$$H(x_2, y_2) = \frac{1}{2}e^{-2y_2} \left( y_2 - x_2^2 + \frac{1}{2} \right), \quad (2.17)$$

In particular, system (2.16) has an equilibrium at  $(0, 0)$  of center type, surrounded by a family of periodic orbits coinciding with the level curves of  $\{H(x, y) = c\}$  for  $c \in (0, \frac{1}{4})$ . The special solution

$$\gamma_{c,2}(t_2) = (x_{c,2}(t_2), y_{c,2}(t_2)) = \left( \frac{1}{2}t_2, \frac{1}{4}t_2^2 - \frac{1}{2} \right), \quad t_2 \in \mathbb{R}. \quad (2.18)$$

separates the periodic orbits from unbounded solutions. Written as a trajectory on the manifold  $B$ , the special solution  $\bar{\gamma}_c$  connects the endpoint  $p_a$  of the critical attracting manifold  $S_a$  across the sphere  $S^2$  to the endpoint  $p_r$  of the critical repelling manifold  $S^r$  (see e.g. [19, Figure 8.2]). In other words, the center manifolds  $\bar{M}_a$  and  $\bar{M}_r$ , corresponding with  $p_a$  and  $p_r$  respectively and written in chart  $K_2$  as  $M_{a,2}$  and  $M_{r,2}$ , intersect along  $\gamma_{c,2}$  for  $r_2 = 0 = \lambda_2$ .

The first order separation between  $M_{a,2}$  and  $M_{r,2}$  with respect to  $r_2$  and  $\lambda_2$  is measured by the distance  $y_{a,2}(0) - y_{r,2}(0)$ , where  $\gamma_{a,2}(t) = (x_{a,2}(t), y_{a,2}(t))$  and  $\gamma_{r,2}(t) = (x_{r,2}(t), y_{r,2}(t))$  are the trajectories in  $M_{a,2}$  and  $M_{r,2}$  respectively for given  $r$  and  $\lambda$  such that  $x_{a,2}(0) = x_{r,2}(0) = 0$ . This distance can be expressed by the function [15, Proposition 3.5]

$$D_c(r_2, \lambda_2) = H(0, y_{a,2}(0)) - H(0, y_{r,2}(0)) = d_r r_2 + d_\lambda \lambda_2 + \mathcal{O}(2), \quad (2.19)$$

where

$$d_r := \int_{-\infty}^{\infty} \text{grad } H(\gamma_{c,2}(t)) \cdot G(\gamma_{c,2}(t)) dt, \quad (2.20)$$

$$d_\lambda := \int_{-\infty}^{\infty} \text{grad } H(\gamma_{c,2}(t)) \cdot \begin{pmatrix} 0 \\ -1 \end{pmatrix} dt \quad (2.21)$$

are the respective Melnikov integrals. Since  $d_\lambda \neq 0$ , one concludes with the implicit function theorem that for  $r$  sufficiently small there is a  $\lambda$  such that the manifolds  $M_{a,2}$  and  $M_{r,2}$  are connected. Transforming back into the original variables yields Theorem 2.1.

*Remark 2.2.* Note that the equation

$$\begin{aligned} x' &= -y + x^2, \\ y' &= \varepsilon x, \end{aligned} \quad (2.22)$$

which is the non-rescaled version of equation (2.16), corresponds with the normal form (2.6) for  $k_3 = k_6 = 0$ ,  $k_1 = k_2 = k_5 = 1$  and  $\lambda = 0$ . In this case, the conserved quantity is given as

$$H(x, y) = \frac{1}{2} e^{-2y/\varepsilon} \left( y - x^2 + \frac{\varepsilon}{2} \right), \quad (2.23)$$

vanishing on the invariant set

$$S_\varepsilon := \left\{ (x, y) \in \mathbb{R}^2 : y = x^2 - \frac{\varepsilon}{2} \right\}, \quad (2.24)$$

which consists precisely of the attracting branch  $S_{a,\varepsilon} = \{(x, y) \in S_\varepsilon : x < 0\}$  and the repelling branch  $S_{r,\varepsilon} = \{(x, y) \in S_\varepsilon : x > 0\}$ , such that trajectories on  $S_\varepsilon$  go through the origin with speed  $\dot{x} = \varepsilon/2$ . Hence, in this case the canard extension exists for any  $\varepsilon > 0$  and we simply have  $\lambda_c(\sqrt{\varepsilon}) = 0$ , in consistency with Theorem 2.1. In particular, this demonstrates that variations of  $\lambda$  are relevant only for perturbations of equation (2.22) according to the general form (2.6).

### 3 Canard extension through a fold in discrete time

In the following, we will investigate what kind of discretization scheme allows for a discrete-time analogon to Theorem 2.1. The existence of the constant of motion (2.17) suggests to apply a discretization method suitable for integrable systems. Before we are going to explore such a scheme, namely the Kahan method, we will demonstrate the shortcomings of an explicit Euler method in this context.

### 3.1 Blow-up

First of all, we introduce the quasi-homogeneous blow-up transformation for the following time-discretizations with step size  $h$  which will also be interpreted as a variable in the full system. Similarly to the ODE problem, the transformation reads

$$x = r\bar{x}, \quad y = r^2\bar{y}, \quad \varepsilon = r^2\bar{\varepsilon}, \quad \lambda = r\bar{\lambda}, \quad h = \bar{h}/r,$$

where  $(\bar{x}, \bar{y}, \bar{\varepsilon}, \bar{\lambda}, r, \bar{h}) \in B := S^2 \times [-\kappa, \kappa] \times [0, \rho] \times [0, h_0]$  for some  $h_0, \rho, \kappa > 0$ . The change of variables in  $h$  is chosen such that the map is desingularized in the relevant charts.

The whole transformation can be formalised as a map  $\Phi : B \rightarrow \mathbb{R}^5$ . When  $P$  denotes the map obtained from the time-discretization, the map  $\Phi$  induces a map  $\bar{P}$  on  $B$  by  $\Phi \circ \bar{P} \circ \Phi^{-1} = P$ . Analogously to the continuous time case, we are using the charts  $K_i$ ,  $i = 1, 2$ , to describe the dynamics. The chart  $K_1$  (setting  $\bar{y} = 1$ ) focuses on the entry and exit of trajectories, and is given by

$$x = r_1x_1, \quad y = r_1^2, \quad \varepsilon = r_1^2\varepsilon_1, \quad \lambda = r_1\lambda_1, \quad h = h_1/r_1. \quad (3.1)$$

In the scaling chart  $K_2$  (setting  $\bar{\varepsilon} = 1$ ) the dynamics arbitrarily close to the origin are analyzed. It is given via the mapping

$$x = r_2x_2, \quad y = r_2^2y_2, \quad \varepsilon = r_2^2, \quad \lambda = r_2\lambda_2, \quad h = h_2/r_2. \quad (3.2)$$

The change of coordinates from  $K_1$  to  $K_2$  is denoted by  $\kappa_{12}$  and, when  $\varepsilon_1 > 0$ , given by

$$x_2 = \varepsilon_1^{-1/2}x_1, \quad y_2 = \varepsilon_1^{-1}, \quad r_2 = r_1\varepsilon_1^{1/2}, \quad \lambda_2 = \varepsilon_1^{-1/2}\lambda_1, \quad h_2 = h_1\varepsilon_1^{1/2}. \quad (3.3)$$

Similarly, when  $y > 0$ , the map  $\kappa_{21} = \kappa_{12}^{-1}$  is given by

$$x_1 = y_2^{-1/2}x_2, \quad r_1 = y_2^{1/2}r_2, \quad \varepsilon_1 = y_2^{-1}, \quad \lambda_1 = y_2^{-1/2}\lambda_2, \quad h_1 = h_2y_2^{1/2}. \quad (3.4)$$

### 3.2 Euler discretization of the canard problem

We apply the explicit Euler discretization to system (2.11), introducing the step size  $h > 0$  of the Euler method as an additional variable. We obtain the map  $P_E : \mathbb{R}^5 \rightarrow \mathbb{R}^5$ , whose iterations  $P_E^n(z_0)$ , for  $n \in \mathbb{N}$  and  $z_0 \in \mathbb{R}^5$ , we are going to analyze close to the origin with  $h, \varepsilon > 0$ , and which is given as

$$P_E : \begin{pmatrix} x \\ y \\ \varepsilon \\ \lambda \\ h \end{pmatrix} \mapsto \begin{pmatrix} \tilde{x} \\ \tilde{y} \\ \tilde{\varepsilon} \\ \tilde{\lambda} \\ \tilde{h} \end{pmatrix} = \begin{pmatrix} x + h(x^2k_2 - yk_1 + \varepsilon k_3) \\ y + \varepsilon h(xk_4 - \lambda k_5 + yk_6) \\ \varepsilon \\ \lambda \\ h \end{pmatrix}, \quad (3.5)$$

where  $k_1, \dots, k_6$  are functions as in (2.7), written without the arguments for simplicity.

Note that by the change of variables  $\varepsilon h \rightarrow h$  we can write the system in the slow time scale as

$$\varepsilon \frac{\tilde{x} - x}{h} = x^2k_2 - yk_1 + \varepsilon k_3, \quad \frac{\tilde{y} - y}{h} = xk_4 - \lambda k_5 + yk_6. \quad (3.6)$$

The critical manifold  $S_0$  is given as

$$S_0 = \left\{ (x, y) \in \mathbb{R}^2 : y = \frac{k_2}{k_1}x^2 \right\},$$



splitting into two normally hyperbolic branches, the attracting subset  $S_a = \{(x, y) \in S_0 : x < 0\}$  and the repelling subset  $S_r = \{(x, y) \in S_0 : x > 0\}$ . It follows from [12, Theorem 4.1] that for  $\varepsilon, h > 0$  small enough there are corresponding forward invariant slow manifolds  $S_{a,\varepsilon,h}$  and  $S_{r,\varepsilon,h}$ . However, note that  $DP_E((0, 0, 0, 0, h)^\top)$  has a quintuple eigenvalue 1 for any  $h \geq 0$ , which means a complete loss of hyperbolicity at the origin as in the ODE case.

We make the following observation:

**Proposition 3.1.** *For  $\lambda = 0$ , the equation of the slow subsystem corresponding with (3.6) reads*

$$\tilde{x}^2 = x^2(1 + hk_6) + xh \frac{k_4 k_1}{k_2},$$

which has the two solutions

$$\tilde{x} = \pm \sqrt{x^2(1 + hk_6) + xh \frac{k_4 k_1}{k_2}}$$

on the set

$$\left\{ (x, y) \in \mathbb{R} \setminus \left( -\frac{hk_4 k_1}{k_2(1 + hk_6)}, 0 \right) \times \mathbb{R} : y = \frac{k_2}{k_1} x^2 \right\} \subset S_0.$$

Each solution has a fixed point at  $x = 0$  as opposed to the continuous-time case where the slow flow follows  $\dot{x} = \frac{1}{2}$ .

*Proof.* Setting  $\varepsilon = 0$  in (3.6), the statement follows from a straight forward calculation.  $\square$

This already indicates that we cannot expect the occurrence of canards for this discretization scheme. Additionally, note that the Euler map (3.5) is not invertible such that Melnikov computations, as desired for proving a similar result to Theorem 2.1 for the discrete time setting, seem not feasible.

However, we will have a look at the scaling chart  $K_2$  in the blown-up system for further clarification. For reasons of clarity, we will ignore the index “2” in the following for all variables. Using 3.2, we observe that  $\tilde{r} = r, \tilde{\lambda} = \lambda, \tilde{h} = h$  and calculate

$$\begin{aligned} \tilde{x}r = \tilde{x} = rx + \frac{h}{r} & \left( -yr^2 k_1(rx, r^2 y, r\lambda, r^2) \right. \\ & \left. + x^2 r^2 k_2(rx, r^2 y, r\lambda, r^2) \right) + r^2 k_3(rx, r^2 y, r\lambda, r^2) \end{aligned}$$

and

$$\begin{aligned} \tilde{y}r^2 = \tilde{y} = r^2 y + hr & \left( xrk_4(rx, r^2 y, r\lambda, r^2) \right. \\ & \left. - \lambda r r k_5(rx, r^2 y, r\lambda, r^2) \right) + yr^2 k_6(rx, r^2 y, r\lambda, r^2) \end{aligned}$$

Hence, we obtain for chart  $K_2$  the map

$$\begin{aligned} \tilde{x} &= x + h(x^2 - y + \mathcal{O}(r)), \\ \tilde{y} &= y + h(x - \lambda + \mathcal{O}(r)). \end{aligned} \tag{3.7}$$

Assume  $\lambda = r = 0$  and recall that the corresponding ODE system (2.16) possesses the first integral  $H$  (2.17) whose zero level set  $\{y = x^2 - \frac{1}{2}\}$  coincides with the trajectory of the special solution  $\gamma$  (2.18) which establishes a canard connection. We cannot expect to find such a conserved quantity for the Euler discretization or, in fact, any other explicit Runge-Kutta method

(cf. [27, Chapter 8]). Accordingly, it follows from an easy calculation that there is no function  $c(h)$  such that  $\{y = x^2 - \frac{1}{2} + c(h)\}$  is invariant for (3.7). In other words, we cannot identify a corresponding candidate for the canard connection. In particular, for  $\lambda = r = 0$ , let  $(x_n, y_n)$  denote a trajectory of (3.7) and assume that for a given  $n \in \mathbb{Z}$  we have  $(x_n, y_n) = (\frac{1}{2}hn, \frac{1}{4}h^2n^2 - \frac{1}{2})$ . Then we observe, in comparison to  $\gamma = (\gamma_1, \gamma_2)$ , that

$$x_{n+1} = \frac{1}{2}h(n+1) = \gamma_1((n+1)h)$$

and

$$y_{n+1} = \frac{1}{4}h^2n^2 - \frac{1}{2} + \frac{1}{2}h^2n = \gamma_2((n+1)h) - \frac{1}{4}h^2.$$

Hence, for  $x_n, y_n > 0$  the trajectory will lie to the right of the parabola  $\gamma$  and jump away from  $\gamma$  in short time, as is illustrated numerically in Figure 1. These observations suggest that, indeed, the Euler scheme is no appropriate discretization for preserving the folded canard phenomenon, as opposed to, for instance, canards through pitchfork or transcritical singularities (cf. [7] and [21]) where no conserved quantity shows up in the scaling chart.

Furthermore, recall from the continuous-time problem that the level sets of the conserved quantity  $H$  (2.17) for  $c \in (0, \frac{1}{4})$  coincide with periodic orbits of (2.16). As already discussed, the Euler scheme does typically not preserve such a conserved quantity and, consequently, also no periodic orbits. Indeed, trajectories of (3.7) above the parabola  $\{y = x^2 - \frac{1}{2}\}$  exhibit spiralling behaviour, as shown in Figure 2. This adds to the evidence that a different discretization scheme is needed for capturing the qualitative behaviour of ODEs with folded canards.

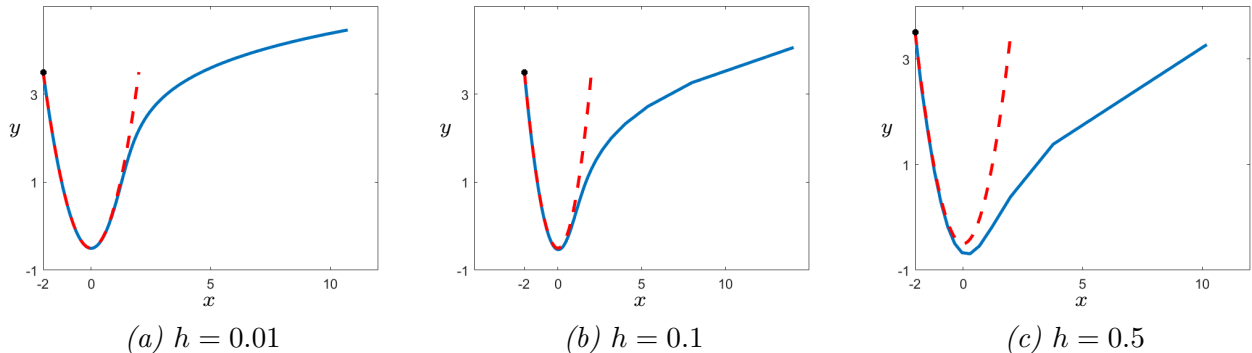


Figure 1: Trajectories of the Euler map in chart  $K_2$  (3.7) for  $\lambda = r = 0$  and different values of  $h$ , starting on a point (black dot) on the curve  $\{y = x^2 - \frac{1}{2}\}$  (red dashed line).

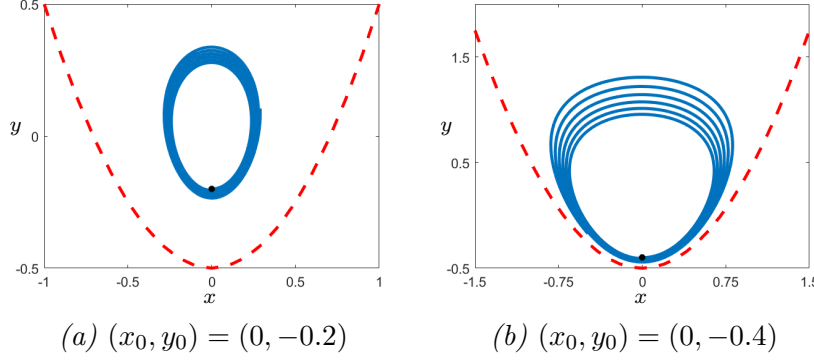


Figure 2: Trajectories of the Euler map in chart  $K_2$  (3.7) for  $\lambda = r = 0$ ,  $h = 0.01$  and different initial points  $(x_0, y_0)$  (black dot) above the curve  $\{y = x^2 - \frac{1}{2}\}$  (red dashed line).

### 3.3 Kahan discretization of canard problem

We discretize system (2.6) with a more suitable method that has produced *integrable* maps in several examples, i.e. maps that conserve a certain quantity: the Kahan-Hirota-Kimura discretization scheme (see e.g. [26]) was introduced by Kahan in the unpublished lecture notes [14] for ODEs with quadratic vector fields

$$\dot{z} = f(z) = Q(z) + Bz + c, \quad (3.8)$$

where each component of  $Q : \mathbb{R}^n \rightarrow \mathbb{R}^n$  is a quadratic form,  $B \in \mathbb{R}^{n \times n}$  and  $c \in \mathbb{R}^n$ . The Kahan-Hirota-Kimura discretization, short *Kahan method*, reads as

$$\frac{\tilde{z} - z}{h} = \bar{Q}(z, \tilde{z}) + \frac{1}{2}B(z + \tilde{z}) + c, \quad (3.9)$$

where

$$\bar{Q}(z, \tilde{z}) = \frac{1}{2}(Q(z + \tilde{z}) - Q(z) - Q(\tilde{z}))$$

is the symmetric bilinear form such that  $\bar{Q}(z, z) = Q(z)$ . Note that equation (3.9) is linear with respect to  $\tilde{z}$  and by that defines a *rational* map  $\tilde{z} = \Lambda_f(z, h)$ , which approximates the time  $h$  shift along the solutions of the ODE (3.8). Further note that  $\Lambda_f^{-1}(z, h) = \Lambda_f(z, -h)$  and, hence, the map is *birational*.

The explicit form of the map  $\Lambda_f$  defined by equation (3.9) is given as

$$\tilde{z} = \Lambda_f(z, h) = z + h \left( \text{Id} - \frac{h}{2} Df(z) \right)^{-1} f(z). \quad (3.10)$$

We will later use this form to analyze a conserved quantity for our problem.

The Kahan method is the specific form, for quadratic vector fields, of an implicit Runge-Kutta scheme which is given by (cf. [2, Proposition 1])

$$\frac{\tilde{z} - z}{h} = -\frac{1}{2}f(z) + 2f\left(\frac{z + \tilde{z}}{2}\right) - \frac{1}{2}f(\tilde{z}). \quad (3.11)$$

Hence, even if the vector field in system (2.11) is non-quadratic, the general scheme (3.11) can be applied. However, we will restrict the following analysis to the quadratic case, so that it

is sufficient to deal with an explicit form of the discretization map (3.10). More precisely, we consider the model

$$\begin{aligned} x' &= -y + x^2 + \varepsilon a_1 x - a_2 xy, \\ y' &= \varepsilon(x - \lambda) + \varepsilon a_5 y + \varepsilon a_4 x^2, \end{aligned} \quad (3.12)$$

which is the normal form (2.6) in the case  $k_1 = 1 + a_2 x$ ,  $k_2 = 1$ ,  $k_3 = a_1 x$ ,  $k_4 = 1 + a_4 x$ ,  $k_5 = 1$ , and  $k_6 = a_5$ . Note that these are the terms that determine the constant  $C$  (2.10) in Theorem 2.1 whose discrete time analogue we are investigating in the following.

Firstly, consider the simplest case, where  $a_1 = a_2 = a_4 = a_5 = 0$ . Then the Kahan discretization of system (3.12)

$$\frac{\tilde{x} - x}{h} = \tilde{x}x - \frac{\tilde{y} + y}{2}, \quad \frac{\tilde{y} - y}{h} = \varepsilon \left( \frac{\tilde{x} + x}{2} - \lambda \right), \quad (3.13)$$

induces the invertible, birational map  $P_K^0 : \mathbb{R}^5 \rightarrow \mathbb{R}^5$ , written explicitly as

$$P_K^0 : \begin{pmatrix} x \\ y \\ \varepsilon \\ \lambda \\ h \end{pmatrix} \mapsto \begin{pmatrix} \tilde{x} \\ \tilde{y} \\ \tilde{\varepsilon} \\ \tilde{\lambda} \\ \tilde{h} \end{pmatrix} = \begin{pmatrix} \frac{x - hy - \frac{h^2}{4}\varepsilon x + \frac{h^2}{2}\lambda\varepsilon}{1 - hx + \frac{h^2}{4}\varepsilon} \\ \frac{y - hyx - \frac{h^2}{2}\varepsilon x^2 - h\lambda\varepsilon + h^2 x \lambda \varepsilon + h\varepsilon x - \frac{h^2}{4}\varepsilon y}{1 - hx + \frac{h^2}{4}\varepsilon} \\ \varepsilon \\ \lambda \\ h \end{pmatrix}. \quad (3.14)$$

The iterations  $(P_K^0)^n(x_0)$ , for  $n \in \mathbb{N}$  and  $x_0 \in \mathbb{R}^5$ , define a dynamical system. Note that by a change of variables  $\varepsilon h \rightarrow h$  we can write the system in the slow time scale as

$$\varepsilon \frac{\tilde{x} - x}{h} = \tilde{x}x - \frac{\tilde{y} + y}{2}, \quad \frac{\tilde{y} - y}{h} = \frac{\tilde{x} + x}{2} - \lambda, \quad (3.15)$$

Similarly to the Euler discretization, one can observe directly from equations (3.15) that the critical manifold  $S_0$  is given as

$$S_0 = \left\{ (x, y) \in \mathbb{R}^2 : y = x^2 \right\},$$

splitting into the attracting branch  $S_a$  and the repelling branch  $S_r$ . Hence, again, there are corresponding forward invariant slow manifolds  $S_{a,\varepsilon,h}$  and  $S_{r,\varepsilon,h}$  for sufficiently small  $\varepsilon, h > 0$ , which also holds for the Kahan map  $P_K$ , derived from the discretization of the general form (2.11). However, note that  $DP_K \left( (0, 0, 0, 0, h)^\top \right)$  has quintuple eigenvalue 1 for any  $h \geq 0$ , which means a complete loss of hyperbolicity at the origin as before.

**Proposition 3.2.** *Setting  $\lambda = 0$  in (3.15), we note that the discrete invariance equation for the slow subsystem gives*

$$\tilde{x}^2 - \frac{h}{2}\tilde{x} = x^2 + \frac{h}{2}x.$$

*Hence, the slow subsystem has the solutions  $\tilde{x} = -x$  and, most notably,  $\tilde{x} = x + \frac{h}{2}$  which is exactly the discretization of the reduced dynamics  $\dot{x} = \frac{1}{2}$  in the ODE case (see equation (2.8) and paragraph below).*

*Proof.* Setting  $\varepsilon = 0$  in (3.15), the statements follow from a simple calculation.  $\square$

We will see later in the analysis of  $P^0$  (3.25), the desingularized version of  $P_K^0$  for  $\lambda = 0$ , that the reduced map  $\tilde{x} = x + \frac{h}{2}$  corresponds with the actual dynamics of the Kahan map. The map  $\tilde{x} = -x$  seems to be an artefact of the underdetermined invariance equation, directly obtained from equations (3.15).

Hence, as opposed to the Euler scheme, the Kahan method gives a trajectory that preserves the slow dynamics through the canard point  $(x_0, y_0) = (0, 0)$ . This already indicates the possible existence of canard solutions for the Kahan discretization.

We take a closer look by applying the blow-up transformation from Section 3.1.

### 3.3.1 Dynamics in entering and exiting chart

Recall from (3.1) that in chart  $K_1$  we have

$$x = r_1 x_1, \quad y = r_1^2, \quad \varepsilon = r_1^2 \varepsilon_1, \quad \lambda = r_1 \lambda_1, \quad h = h_1 / r_1, \quad (3.16)$$

where  $0 \leq r_1 \leq \rho$ ,  $0 \leq \varepsilon \leq \varepsilon_0 / \rho^2 =: \delta$  and  $0 \leq h_1 \leq \nu$  for  $\nu, \delta > 0$  sufficiently small, in particular  $\nu < 1$ . In other words, we consider the domain

$$D_1 := \left\{ (x_1, r_1, \varepsilon_1, \lambda_1, h_1) \in \mathbb{R}^5 : 0 \leq r_1 \leq \rho, 0 \leq \varepsilon_1 \leq \delta, 0 \leq h_1 \leq \nu \right\}. \quad (3.17)$$

Note that, transforming the map (3.14) into the coordinates of  $K_1$ , we can treat the potential additional terms involving  $a_1, a_2, a_4, a_5$  as  $\mathcal{O}(r_1)$  and  $\mathcal{O}(\varepsilon_1 r_1)$  respectively, vanishing in the case of (3.14).

We introduce the functions

$$F(x_1, \varepsilon_1, \lambda_1, h_1) = 1 - h_1 x_1 + h_1 \varepsilon_1 x_1 - \frac{h_1^2}{2} \varepsilon_1 x_1^2 - h_1 \lambda_1 \varepsilon_1 + h_1^2 x_1 \lambda_1 \varepsilon_1 - \frac{h_1^2}{4} \varepsilon_1,$$

$$E(x_1, \varepsilon_1, h_1) = 1 - h_1 x_1 + \frac{h_1^2}{4} \varepsilon_1,$$

and

$$G(x_1, r_1, \varepsilon_1, \lambda_1, h_1) = \frac{F(x_1, \varepsilon_1, \lambda_1, h_1)}{E(x_1, \varepsilon_1, h_1)} + \mathcal{O}(\varepsilon_1 r_1).$$

We can derive the maps for each variable in chart  $K_1$  leading to the following desingularized dynamics:

$$\begin{aligned} \tilde{x}_1 &= \frac{x_1 - h_1 - \frac{h_1^2}{4} \varepsilon_1 x_1 + \frac{h_1^2}{2} \lambda_1 \varepsilon_1}{F_1(x_1, \varepsilon_1, \lambda_1, h_1)^{1/2} E(x_1, \varepsilon_1, h_1)^{1/2}} + \mathcal{O}(r_1), \\ \tilde{r}_1 &= r_1 G(x_1, r_1, \varepsilon_1, \lambda_1, h_1)^{1/2}, \\ \tilde{\varepsilon}_1 &= \varepsilon_1 G_1(x_1, r_1, \varepsilon_1, \lambda_1, h_1)^{-1}, \\ \tilde{\lambda}_1 &= \lambda_1 G_1(x_1, r_1, \varepsilon_1, \lambda_1, h_1)^{-1/2}, \\ \tilde{h}_1 &= h_1 G_1(x_1, r_1, \varepsilon_1, \lambda_1, h_1)^{1/2}. \end{aligned} \quad (3.18)$$

On the invariant subset  $\{r_1 = 0, \varepsilon_1 = 0, \lambda_1 = 0\} \subset D_1$ , we have that  $G(x_1, r_1, \varepsilon_1, \lambda_1, h_1) = 1$  and observe that in this case

$$\tilde{x}_1 = \frac{x_1 - h_1}{1 - h_1 x_1}, \quad \tilde{h}_1 = h_1.$$

Hence, there are the two fixed points

$$p_{a,1}(h_1) = (-1, 0, 0, 0, h_1) \quad \text{and} \quad p_{r,1}(h_1) = (1, 0, 0, 0, h_1),$$

with  $x_1$ -derivatives

$$1 \geq \left| \frac{1-h_1}{1+h_1} \right| = |D_{x_1} \tilde{x}_1(p_{a,1}(h_1))| =: \alpha, \quad 1 \leq \left| \frac{1+h_1}{1-h_1} \right| = |D_{x_1} \tilde{x}_1(p_{r,1}(h_1))| = \frac{1}{\alpha}.$$

Recall that we have  $h_1 \leq \nu < 1$ .

While for  $h_1 > 0$  we have  $\alpha < 1$  such that the point  $p_{a,1}(h_1)$  is attracting and the point  $p_{r,1}(h_1)$  repelling in  $x_1$ -direction, it is easy to see that all derivatives with respect to the other variables equal 1 at these fixed points.

For small  $r_1 > 0$  on  $\{\varepsilon_1 = 0, \lambda_1 = 0\} \subset D_1$  we obtain

$$\tilde{x}_1 = \frac{x_1 - h_1}{1 - h_1 x_1} + \mathcal{O}(r_1), \quad \tilde{h}_1 = h_1, \quad \tilde{r}_1 = r_1.$$

Hence, using the implicit function theorem, we can conclude the existence of two families of, for  $h_1 > 0$  normally hyperbolic, curves of fixed points written as  $S_{a,1}(h_1)$  and  $S_{r,1}(h_1)$  on  $\{\varepsilon_1 = 0, \lambda_1 = 0\} \subset D_1$ , where, at  $r_1 = 0$ ,  $p_{j,1}(h_1)$  is the endpoint of  $S_{j,1}(h_1)$  for  $j = a, r$ . In the situation of (3.14), where the  $\mathcal{O}(r_1)$ -term vanishes, these are simply given by the lines

$$S_{a,1}(h_1) = \{(-1, r_1, 0, 0, h_1) : 0 \leq r_1 \leq \rho\} \subset D_1 \quad \text{and} \quad S_{r,1}(h_1) = \{(1, r_1, 0, 0, h_1) : 0 \leq r_1 \leq \rho\} \subset D_1.$$

On the invariant set  $\{r_1 = 0, \lambda_1 = 0\} \subset D_1$ , the dynamics of  $x_1$ ,  $\varepsilon_1$  and  $h_1$  satisfy

$$\begin{aligned} \tilde{x}_1 &= \frac{x_1 - h_1 - \frac{h_1^2}{4} \varepsilon_1 x_1}{(1 - h_1 x_1 + h_1 \varepsilon_1 x_1 - \frac{h_1^2}{2} \varepsilon_1 x_1^2 - \frac{h_1^2}{4} \varepsilon_1)^{1/2} (1 - h_1 x_1 + \frac{h_1^2}{4} \varepsilon_1)^{1/2}}, \\ \tilde{\varepsilon}_1 &= \varepsilon_1 \frac{1 - h_1 x_1 + \frac{h_1^2}{4} \varepsilon_1}{1 - h_1 x_1 + h_1 \varepsilon_1 x_1 - \frac{h_1^2}{2} \varepsilon_1 x_1^2 - \frac{h_1^2}{4} \varepsilon_1}, \\ \tilde{h}_1 &= h_1 \left( \frac{1 - h_1 x_1 + h_1 \varepsilon_1 x_1 - \frac{h_1^2}{2} \varepsilon_1 x_1^2 - \frac{h_1^2}{4} \varepsilon_1}{1 - h_1 x_1 + \frac{h_1^2}{4} \varepsilon_1} \right)^{1/2}. \end{aligned} \tag{3.19}$$

We compute the Jacobians of the map (3.19) at  $p_{a,1}(h_1)$  and  $p_{r,1}(h_1)$ , restricting to the invariant set  $\{r_1 = 0, \lambda_1 = 0\} \subset D_1$ ,

$$\begin{aligned} \frac{\partial(\tilde{x}_1, \tilde{\varepsilon}_1, \tilde{h}_1)}{\partial(x_1, \varepsilon_1, h_1)}((-1, 0, h_1)) &= \begin{pmatrix} \frac{1-h_1}{1+h_1} & \frac{-h_1}{2(1+h_1)} & 0 \\ 0 & 1 & 0 \\ 0 & -\frac{h_1^2}{2} & 1 \end{pmatrix}, \\ \frac{\partial(\tilde{x}_1, \tilde{\varepsilon}_1, \tilde{h}_1)}{\partial(x_1, \varepsilon_1, h_1)}((1, 0, h_1)) &= \begin{pmatrix} \frac{1+h_1}{1-h_1} & \frac{-h_1}{2(1-h_1)} & 0 \\ 0 & 1 & 0 \\ 0 & \frac{h_1^2}{2} & 1 \end{pmatrix}. \end{aligned}$$

Hence, for the vectors  $v_a = (-1, 4, 1)^\top$  and  $v_r = (-1, -4, -1)^\top$  we have

$$\begin{aligned} \frac{\partial(\tilde{x}_1, \tilde{\varepsilon}_1, \tilde{h}_1)}{\partial(x_1, \varepsilon_1, h_1)}((-1, 0, h_1)) v_a &= v_a + (0, 0, -2h_1^2)^\top, \\ \frac{\partial(\tilde{x}_1, \tilde{\varepsilon}_1, \tilde{h}_1)}{\partial(x_1, \varepsilon_1, h_1)}((1, 0, h_1)) v_r &= v_r + (0, 0, 2h_1^2)^\top. \end{aligned}$$

This shows that along the  $\varepsilon_1$  and  $x_1$ -direction the linearization has the identical eigenvector to the continuous-time case (see e.g [15, Lemma 2.5]) but that there is additionally the infinitesimal decrease in  $h_1$  at  $p_{a,1}(h_1)$  and increase in  $h_1$  at  $p_{r,1}(h_1)$ .

We conclude the existence of the two-dimensional center manifolds  $N_{a,1}$  and  $N_{r,1}$ , parametrized in  $h_1, \varepsilon_1$ , that at  $\varepsilon_1 = 0$  coincide with

$$P_{a,1} = \{p_{a,1}(h_1) : 0 \leq h_1 \leq \nu\} \text{ and } P_{r,1} = \{p_{r,1}(h_1) : 0 \leq h_1 \leq \nu\} \quad (3.20)$$

respectively (see Figure 3 (b)). Note from (3.19) that on  $\{r_1 = 0, \lambda_1 = 0, h_1 > 0\} \subset D_1$  we have  $\tilde{\varepsilon}_1 > \varepsilon_1$  and  $\tilde{h}_1 < h_1$  for  $x_1 \leq 0$ . Hence, for  $\delta$  small enough, the branch of the manifold  $N_{a,1}$  on  $\{r_1 = 0, \varepsilon_1 > 0, \lambda_1 = 0, h_1 > 0\} \subset D_1$  is unique. On the other hand, introducing a constant  $K > 0$ , we observe that for  $\frac{1}{K} \leq x_1$  we have  $\tilde{\varepsilon}_1 < \varepsilon_1$  and  $\tilde{h}_1 > h_1$ , if and only if  $h_1 < \frac{2K}{1+K^2}$ . Setting  $K > 1$  for the case of  $x_1$  taken from a neighbourhood of 1, we obtain  $\nu < \frac{2K}{1+K^2} < 1$  in order to guarantee that, for  $\delta$  small enough depending on  $K$ , the branch of the manifold  $N_{r,1}$  on  $\{r_1 = 0, \varepsilon_1 > 0, \lambda_1 = 0, h_1 > 0\} \subset D_1$  is unique.

We summarize these observations into the following Proposition:

**Proposition 3.3.** *For system (3.18) there exist a center-stable manifold  $\hat{M}_{a,1}$  and a center-unstable manifold  $\hat{M}_{r,1}$ , originating at the sets of fixed points  $P_{a,1}$  and  $P_{r,1}$  (3.20) respectively, with the following properties:*

1. *For  $i = a, r$ , the manifold  $\hat{M}_{i,1}$  contains the curve of fixed points  $S_{i,1}(h_1)$  on  $\{\varepsilon_1 = 0, \lambda_1 = 0\} \subset D_1$ , parametrized in  $r_1$ , and the center manifold  $N_{i,1}$  whose branch for  $\varepsilon_1, h_1 > 0$  is unique (see Figure 3 (b)). In  $D_1$ , the manifold  $\hat{M}_{i,1}$  is given as a graph  $x_1 = \hat{g}_i(r_1, \varepsilon_1, \lambda_1, h_1)$ .*
2. *The invariances  $\tilde{r}_1 \tilde{\lambda}_1 = r_1 \lambda_1$  and  $\tilde{h}_1 / \tilde{r}_1 = h_1 / r_1$  imply the existence of a two-dimensional invariant manifold  $M_{i,1}$  which is given as a graph  $x_1 = g_i(r_1, \varepsilon_1)$ .*

*Proof.* The first part follows immediately from the above considerations and standard center manifold theory. The second part follows as in [7] (see [7, Proposition 3.3 and Figure 2] for details).  $\square$

We will now investigate the dynamics in the rescaling chart  $K_2$  in order to find a special canard trajectory connecting  $\hat{M}_{a,1}$  and  $\hat{M}_{r,1}$  or  $M_{a,1}$  and  $M_{r,1}$  respectively.

### 3.3.2 Dynamics in rescaling chart

Recall from (3.2) that in chart  $K_2$  we have

$$x = r_2 x_2, \quad y = r_2^2 y_2, \quad \varepsilon = r_2^2, \quad \lambda = r_2 \lambda_2, \quad h = h_2 / r_2. \quad (3.21)$$

Since in this chart  $r_2 = \sqrt{\varepsilon}$  is not a dynamical variable (remains fixed in time), we will not write down explicitly differential, resp. difference evolution equations for  $\lambda_2 = \lambda / \sqrt{\varepsilon}$  and for  $h_2 = h \sqrt{\varepsilon}$ . We will restore these variables as we come to the matching with the chart  $K_1$ . Starting from here, we omit index “2” referring to the chart  $K_2$ . In particular, we write  $x, y, r, \lambda, h$  for  $x_2, y_2, r_2, \lambda_2, h_2$  rather than for original variables (before rescaling). We observe that, in chart  $K_2$ , equation (3.12) takes the form

$$\begin{aligned} x' &= -y + x^2 + r(a_1 x - a_2 x y), \\ y' &= x - \lambda + r(a_4 x^2 + a_5 y). \end{aligned} \quad (3.22)$$

Comparing the coordinate transformations (2.13) and (3.21), it is easy to observe that in chart  $K_2$  the Kahan map corresponding with the model system (3.12) is precisely the Kahan discretization of equation (3.22) and can be written as

$$\begin{aligned}\tilde{x} &= P_1^0(x, y, h) + r\hat{G}_1(x, y, h) + \lambda\hat{J}_1(x, h), \\ \tilde{y} &= P_2^0(x, y, h) + r\hat{G}_2(x, y, h) + \lambda\hat{J}_2(x, h).\end{aligned}\quad (3.23)$$

In order to make (3.23) explicit, we first consider the case  $a_1 = a_2 = a_4 = a_5 = 0$ . Then in original coordinates the Kahan map is  $P_K^0$  (3.14) and in rescaled coordinates of  $K_2$  (3.21) this yields

$$\begin{aligned}\tilde{x} &= \frac{x - hy - \frac{h^2}{4}x + \frac{h^2}{2}\lambda}{1 - hx + \frac{h^2}{4}}, \\ \tilde{y} &= \frac{y - hyx - \frac{h^2}{2}x^2 - h\lambda + h^2x\lambda + hx - \frac{h^2}{4}y}{1 - hx + \frac{h^2}{4}}.\end{aligned}\quad (3.24)$$

Hence, we observe from (3.24) that  $P^0 = (P_1^0, P_2^0)$  is given by

$$P^0(x, y, h) = \left( \begin{array}{c} \frac{x - hy - \frac{h^2}{4}x}{1 - hx + \frac{h^2}{4}} \\ \frac{y - hyx - \frac{h^2}{2}x^2 + hx - \frac{h^2}{4}y}{1 - hx + \frac{h^2}{4}} \end{array} \right), \quad (3.25)$$

and we have

$$\hat{J}_1(x, h) = \frac{\frac{h^2}{2}}{1 - hx + \frac{h^2}{4}}, \quad \hat{J}_2(x, h) = \frac{h^2x - h}{1 - hx + \frac{h^2}{4}}. \quad (3.26)$$

The functions  $\hat{G}_1$  and  $\hat{G}_2$  will generally look very complicated and we refrain from giving general formulas here. We will give an example at the end for illustration of our results.

### Invariant density and invariant curve

Similarly to the continuous-time case, we start the analysis in  $K_2$  with the case  $\lambda = 0$ ,  $r = 0$  for  $h > 0$  fixed. This means that we study the dynamics of the map  $P^0$  (3.25).

As opposed to the Euler scheme, we can actually find an invariant curve for (3.25) which deviates from the invariant parabola in the continuous time case by a function  $c(h)$ . In more detail, we have the following statements:

**Proposition 3.4.** *The parabola*

$$S_h := \left\{ (x, y) \in \mathbb{R}^2 : y = x^2 - \frac{1}{2} - \frac{h^2}{8} \right\} \quad (3.27)$$

is invariant under iterations of  $P^0$  (3.25). Solutions on  $S_h$  are given by

$$\gamma_{h, x(0)}(n) = \left( x(0) + h\frac{n}{2}, x(0)^2 + 2hnx(0) + h^2\frac{n^2}{4} - \frac{1}{2} - \frac{h^2}{8} \right) \quad \text{for all } n \in \mathbb{Z},$$

denoting, for  $x(0) = 0$ ,

$$\gamma_h(n) = \left( h\frac{n}{2}, h^2\frac{n^2}{4} - \frac{1}{2} - \frac{h^2}{8} \right) \quad \text{for all } n \in \mathbb{Z}. \quad (3.28)$$



In particular, for  $(x, y) \in S_h$  we have:

$$\left| \frac{\partial \tilde{x}}{\partial x} \right| \begin{cases} < 1 & \text{as long as } x < 0, \\ = 0 & \text{for } x = 0, \\ > 1 & \text{as long as } x > 0, x \neq \left(1 + \frac{h^2}{4}\right)/h. \end{cases}$$

*Proof.* The invariance of  $S_h$  follows from an easy calculation. Furthermore, observe that if  $(x, y) \in S_h$ , we have

$$\tilde{x} = \frac{x - hx^2 + \frac{h}{2} + \frac{h^3}{8} - \frac{h^2}{4}x}{1 - hx + \frac{h^2}{4}} = \frac{\left(1 - hx + \frac{h^2}{4}\right)\left(x + \frac{h}{2}\right)}{1 - hx + \frac{h^2}{4}} = x + \frac{h}{2}.$$

We compute the Jacobian matrix associated with (3.25) as

$$\frac{\partial(\tilde{x}, \tilde{y})}{\partial(x, y)} = \begin{pmatrix} \frac{1 - h^2 y - \frac{h^4}{16}}{\left(1 - hx + \frac{h^2}{4}\right)^2} & -\frac{h}{1 - hx + \frac{h^2}{4}} \\ \frac{h - h^2 x + \frac{h^3}{4}(2x^2 - 2y + 1) - \frac{h^4}{4}x}{\left(1 - hx + \frac{h^2}{4}\right)^2} & \frac{1 - hx - \frac{h^2}{4}}{1 - hx + \frac{h^2}{4}} \end{pmatrix}. \quad (3.29)$$

In particular, observe that for  $(x, y) \in S_h$  we have

$$\frac{\partial \tilde{x}}{\partial x}(x, y) = \frac{-h^2 x^2 + \left(1 + \frac{h^2}{4}\right)^2}{h^2 x^2 - x\left(2h + \frac{h^3}{2}\right) + \left(1 + \frac{h^2}{4}\right)^2} =: \frac{f_h(x)}{g_h(x)}.$$

The claim for  $x \leq 0$  can be deduced directly from this form. For  $x > 0$ , note that  $f_h(x)$  and  $g_h(x)$  both have exactly one root, namely at  $x^* = \left(1 + \frac{h^2}{4}\right)/h$ . Since  $g_h(x) \rightarrow \infty$  as  $x \rightarrow \infty$  we can conclude that  $g_h(x)$  stays nonnegative, while  $f_h(x)$  obviously changes sign at  $x^*$ . Hence, we observe for  $xh < 1 + \frac{h^2}{4}$  that

$$|f_h(x)| - |g_h(x)| = 2hx + \frac{h^3}{2}x - 2h^2 x^2 > 0.$$

For  $xh > 1 + \frac{h^2}{4}$  we have that

$$|f_h(x)| - |g_h(x)| = 2hx + hx\frac{h^2}{2} - 2\left(1 + \frac{h^2}{4}\right)^2 > 2\left(1 + \frac{h^2}{4}\right) + \left(1 + \frac{h^2}{4}\right)\frac{h^2}{2} - 2\left(1 + \frac{h^2}{4}\right)^2 = 0.$$

This concludes the claim.  $\square$

The trajectory  $\gamma_h$  is shown in global blow-up coordinates as  $\gamma_{\bar{h}}$  in Figure 3 (a), in comparison to the ODE trajectory  $\bar{\gamma}_c$  corresponding with  $\gamma_{c,2}$  in  $K_2$ . The invariant set  $S_h$  (3.27), and the trajectories thereon, can be assumed to play the role of a separatrix for iterations of  $P^0$  (3.25) between bounded orbits, which lie above  $S_h$ , and unbounded orbits, which lie below  $S_h$ . This behaviour is illustrated in Figures 4, 5, 7 and 6, and further discussed in the paragraph beneath Figure 4.

*Remark 3.5.* Note that, when  $\lambda = 0$ , the map  $P_K^0$  (3.14) is the non-rescaled version of  $P^0$  (3.25) and has the invariant curve

$$S_{h,\varepsilon} := \left\{ (x, y) \in \mathbb{R}^2 : y = x^2 - \frac{\varepsilon}{2} - \frac{\varepsilon^2 h^2}{8} \right\}. \quad (3.30)$$

In particular, the map  $P_K^0$  (3.14) is the Kahan discretization of equation (2.22), as discussed in Remark 2.2. Analogously, we observe that  $S_{h,\varepsilon}$  consists of the attracting branch  $S_{a,\varepsilon,h} = \{(x, y) \in S_{h,\varepsilon} : x < 0\}$  and the repelling branch  $S_{r,\varepsilon,h} = \{(x, y) \in S_{h,\varepsilon} : x > 0\}$ , such that trajectories on  $S_{h,\varepsilon}$  go through the origin with speed  $\tilde{x} = x + \frac{h\varepsilon}{2}$ . Hence, in this situation the canard extension exists for any  $\varepsilon > 0$  and we simply have  $\lambda_c^h(\sqrt{\varepsilon}) = 0$ , as in continuous time. Variations of  $\lambda$  will become significant for the Kahan discretization of the more general form (3.12), as we will make precise in Theorem 3.10.

We can show the following connection to the chart  $K_1$ :

**Lemma 3.6.** *The trajectory  $\gamma_h(n)$ , transformed into the chart  $K_1$  via*

$$\gamma_h^1(n) = \kappa_{21}(\gamma_h(n), h)$$

for large  $|n|$ , lies in  $\hat{M}_{a,1}$  as well as  $\hat{M}_{r,1}$ .

*Proof.* Observe from (3.4) that for  $|n|$  large enough the component  $\varepsilon_1(n)$  of  $\gamma_h^1(n)$  is sufficiently small such that  $\gamma_h^1$ , which lies on the invariant manifold  $\kappa_{21}(S_h, h)$ , has to be on  $N_{a,1}$  for  $n < 0$ , and  $N_{r,1}$  for  $n > 0$  respectively, due to the uniqueness of the invariant manifold (see Proposition 3.3). In particular, observe that, by taking  $h$  small enough,  $\gamma_h^1$  reaches an arbitrarily close vicinity of some  $p_{a,1}(h_1^*)$  for sufficiently small  $n < 0$  and  $p_{r,1}(h_1^*)$  for sufficiently large  $n > 0$ , within  $N_{a,1} \subset \hat{M}_{a,1}$  and  $N_{r,1} \subset \hat{M}_{r,1}$  respectively (see also Figure 3 (b)). This finishes the proof.  $\square$

Moreover, we define the function

$$\varphi_h(x, y) := x^2 - y - \frac{1}{2} - \frac{h^2}{8},$$

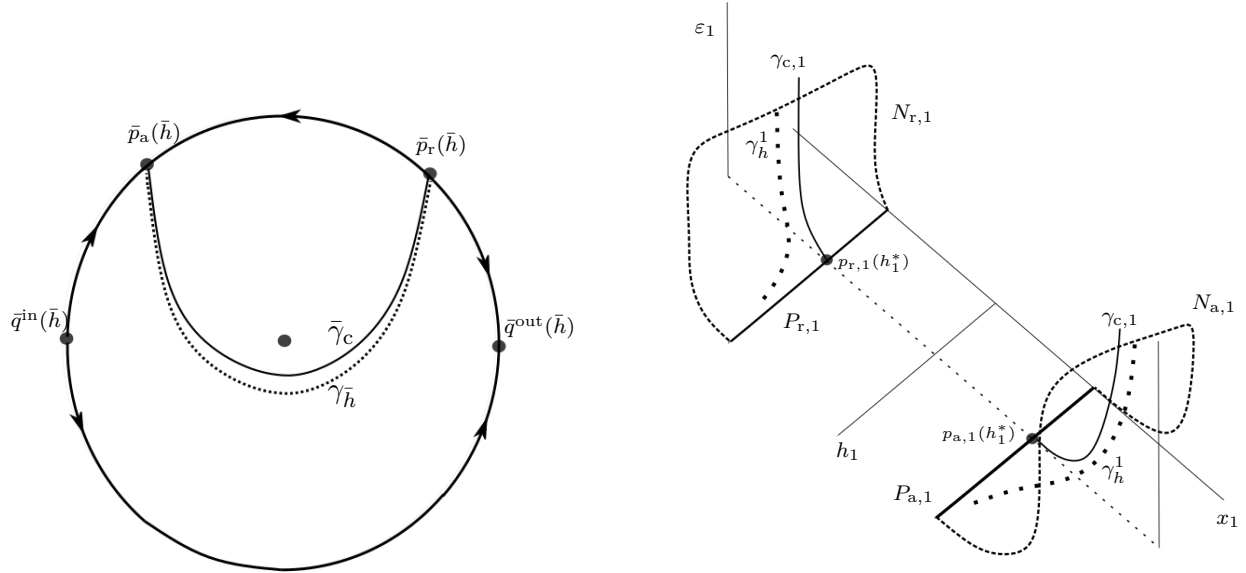
and observe that for  $P^0$  (3.25) we have

$$\det D_{x,y}(\tilde{x}, \tilde{y})(x, y) = \frac{\varphi_h(\tilde{x}, \tilde{y})}{\varphi_h(x, y)}.$$

Hence, we can conclude that the measures

$$\mu_h^\pm(dx, dy) = \frac{1}{\pm\varphi_h(x, y)} dx dy \quad (3.31)$$

are invariant measures for the map  $P^0$  (3.25), where  $\mu_h^-$  is defined on  $\mathcal{B}\left(\left\{y > x^2 - \frac{1}{2} - \frac{h^2}{8}\right\}\right)$  and  $\mu_h^+$  is defined on  $\mathcal{B}\left(\left\{y < x^2 - \frac{1}{2} - \frac{h^2}{8}\right\}\right)$ . Observe that both measures become singular on  $S_h$ , similarly to the continuous-time case where the invariant densities  $\frac{1}{\pm\varphi(x,y)}$  are singular on  $\left\{y = x^2 - \frac{1}{2}\right\}$  (see Appendix A.1).



(a) Dynamics on  $S^{2,+} \times \{0\} \times \{0\} \times \{\bar{h}\}$ , where  $S^{2,+}$  denotes the upper hemisphere

(b) Dynamics in  $K_1$  for  $r_1 = \lambda_1 = 0$

Figure 3: The trajectory  $\gamma_{\bar{h}}$  in global blow-up coordinates for  $r = \bar{\lambda} = 0$  and  $\bar{h} > 0$  fixed (a) and as  $\gamma_{\bar{h}}^1$  in  $K_1$  for  $r_1 = \lambda_1 = 0$  (b). The figures also show the special ODE solution  $\bar{\gamma}_c$  connecting  $\bar{p}_r(\bar{h})$  and  $\bar{p}_a(\bar{h})$  (a) and  $\gamma_{c,1}$  connecting  $p_{a,1}(h_1^*)$  and  $p_{r,1}(h_1^*)$  for fixed  $h_1^* > 0$  (b) respectively. In Figure (a), the fixed points  $\bar{q}^{\text{in}}(\bar{h})$  and  $\bar{q}^{\text{out}}(\bar{h})$ , for  $\bar{\varepsilon} = 0$ , are added, whose existence can be seen in an extra chart, analogously to before (see [15]). In Figure (b), the trajectory  $\gamma_{\bar{h}}^1$  is shown on the attracting center manifold  $N_{a,1} \subset \hat{M}_{a,1}$  and the repelling center manifold  $N_{r,1} \subset \hat{M}_{r,1}$  (see Section 3.3.1 and Lemma 3.6).

### Formal conserved quantity

Recall from (2.17) that, for  $r = \lambda = 0$ , the ODE system (2.16) in chart  $K_2$  has the conserved quantity

$$H(x, y) = \frac{1}{2} e^{-2y} \left( y - x^2 + \frac{1}{2} \right),$$

with the special canard solution (2.18) given by

$$\gamma_{c,2}(t_2) = \left( \frac{1}{2} t_2, \frac{1}{4} t_2^2 - \frac{1}{2} \right),$$

which satisfies  $H(\gamma_{c,2}(t_2)) = 0$  for all  $t_2 \in \mathbb{R}$ . Due to the fact that the Kahan discretization allows for a conserved quantity in several examples of quadratic vector fields, we try to find a constant of motion for the map  $P^0$  (3.25) as the time discretization of (2.16).

In Appendix A.2, we derive an Ansatz for finding a formal conserved quantity via a series expansion which is then a candidate for a finite first integral of the map. Following this approach, we obtain the formal conserved quantity  $\bar{H}(x, y, h)$  for (3.25), which can be written as

$$\bar{H}(x, y, h) = H(x, y) + e^{-2y} \sum_{i \geq 1} h^{2i} \sum_{k=2}^{2(i+1)} H_k(x, y), \quad (3.32)$$

where the  $H_k(x, y)$  turn out to be polynomials of degree  $k$ . However, beware that this is only a formal series and convergence to a smooth function as a conserved quantity is not clear a priori.

We denote

$$\bar{H}_{2i}(x, y) = \sum_{k=2}^{2(i+1)} H_k(x, y),$$

and demonstrate the computation of  $\bar{H}_2$  according to the derivation in Appendix A.2. A Taylor expansion of  $H(\tilde{x}, \tilde{y})$  as in (A.6) gives

$$H(\tilde{x}, \tilde{y}) = H(x, y) + h^3 G_3(x, y) + \mathcal{O}(h^4),$$

with

$$G_3(x, y) = \frac{1}{6} e^{-2y} x(x^2 + x^4 - 4x^2 y + 3y^2).$$

Hence, we can obtain  $\bar{H}_2$  by solving (up to a formal integral) equation (A.8), which in our case reads

$$G_3(x, y) = - \left( (x^2 - y) \frac{\partial}{\partial x} (\bar{h}(x, y) e^{-2y}) + x \frac{\partial}{\partial y} (\bar{h}(x, y) e^{-2y}) \right). \quad (3.33)$$

Assuming  $\bar{H}_2$  to be polynomial and comparing coefficients gives

$$\bar{h}(x, y) = \frac{1}{6} \left( \frac{1}{2} + y(1 + y - y^2) - x^2 \left( \frac{x^2}{2} + y - y^2 \right) \right). \quad (3.34)$$

Hence, we obtain the approximation

$$\bar{H}(x, y, h) = H(x, y) + \frac{h^2}{6} e^{-2y} \left( \frac{1}{2} + y(1 + y - y^2) - x^2 \left( \frac{x^2}{2} + y - y^2 \right) \right) + \mathcal{O}(h^4). \quad (3.35)$$

We will turn to a numerical exploitation of this approximation below. Firstly, we consider the potential existence of a separating solution similarly to  $\gamma_{c,2}$  (2.18). Let  $X := C^1(I, \mathbb{R})$  denote the space of continuously differentiable functions from  $I$  to  $\mathbb{R}$ , which is a Banach space with the usual supremum norm. We define the map  $\tilde{F} : \mathbb{R} \times X \rightarrow X$

$$\tilde{F}(h, f(\cdot)) = \bar{H}(\cdot, f(\cdot), h) \quad \text{for all } h \in \mathbb{R}, f \in X. \quad (3.36)$$

The following Proposition then implies the existence of an invariant curve for (3.25) living on the zero level set of  $\bar{H}$  in case it exists:

**Proposition 3.7.** *If  $\bar{H}$  as given in (3.32) is a well-defined function such that  $\tilde{F}$  (3.36) is continuously Frechet differentiable, then for any compact interval  $I \subset \mathbb{R}$  there is a  $h_I > 0$  such that for all  $h \in [0, h_I]$  there is a continuously differentiable  $g_h : I \rightarrow \mathbb{R}$  with*

$$\bar{H}(x, g_h(x), h) = 0 \quad \text{for all } x \in I,$$

and  $g_h \rightarrow g_0$  in  $X$  as  $h \rightarrow 0$  where  $g_0 : I \rightarrow \mathbb{R}$  is given by  $g_0(x) = x^2 - \frac{1}{2}$ .

*Proof.* Firstly, observe that  $\tilde{F}(0, g_0(\cdot)) \equiv 0$ . We denote the Frechet derivative of  $\tilde{F}$  by  $d\tilde{F}$ . We can apply the Implicit Function Theorem for Banach spaces and, by that, deduce the statements in the Proposition if the map

$$\eta \mapsto D\tilde{F}(0, g_0)(0, \eta) \quad (3.37)$$

is an isomorphism from  $X$  to  $X$ . Indeed, the Frechet derivative in (3.37) can be computed to be

$$\begin{aligned}
D\tilde{F}(0, g_0(x))(0, \eta) &= \lim_{\varepsilon \rightarrow 0} \frac{\tilde{F}(0, g_0(x) + \varepsilon\eta(x)) - \tilde{F}(0, g_0)}{\varepsilon} \\
&= \left[ \frac{\partial}{\partial \varepsilon} \left[ \frac{1}{2} e^{-2(g_0(x) + \varepsilon\eta(x))} \left( g_0(x) + \varepsilon\eta(x) - x^2 + \frac{1}{2} \right) \right] \right]_{\varepsilon=0} \\
&= \left[ \frac{1}{2} e^{-2(g_0(x) + \varepsilon\eta(x))} \left( -2\eta(x) \left( g_0(x) + \varepsilon\eta(x) - x^2 + \frac{1}{2} \right) + \eta(x) \right) \right]_{\varepsilon=0} \\
&= \frac{e}{2} e^{-2x^2} \eta(x).
\end{aligned}$$

Hence, the map (3.37) is clearly an isomorphism from  $X$  to  $X$  and the statement follows.  $\square$

Note that, naturally, from Proposition 3.4, the function  $y = x^2 - \frac{1}{2} - \frac{h^2}{8}$  is a candidate for  $g_h$  in Proposition 3.7, such that the special solution  $\gamma_h$  (3.28) satisfies  $\bar{H}(\gamma_h, h) = 0$ .

Since we cannot find a closed formula for  $\bar{H}$  or even show its convergence analytically, we test our theoretical considerations above against numerical computations of trajectories for (3.25). Firstly, we consider different initial points  $(x_{2,0}, y_{2,0})$  for  $x_{2,0} = 0$  and  $y_{2,0} \in \left(-\frac{1}{2}, 0\right)$ . Similarly to the time-continuous system (2.16) and in contrast to the Euler discretization (see Figure 2), we observe periodic behaviour in Figure 4. The pictures in the first row show the trajectories (blue line) above  $S_h$  (3.27) (red dashed line) while the figures in the second row show the corresponding values of  $\bar{H}$  as approximated in (3.35) (blue line) compared to the values of the first integral  $H$  (red dashed line), along the trajectories. Note that in every example our approximations of  $\bar{H}$  are constant – up to the displayed precision – along trajectories, as opposed to  $H$ . This suggests that some  $\bar{H}$  indeed exists as a constant of motion under (3.25) and is approximated well by (3.35).

We observe the same evidence for the conserved quantity  $\bar{H}$  when we investigate trajectories starting on a point of  $\gamma_{c,2}$  (2.18), the solution of the ODE (2.16) which separates bounded and unbounded solutions and satisfies  $H(\gamma_{c,2}) = 0$ . Again in contrast to the Euler discretization (see Figure 1), we observe in Figure 5 that trajectories stay close to  $\gamma_{c,2}$  for long times connecting the repelling and attracting branches of the parabola with periodic behaviour. Since  $\gamma_{c,2}$  lies above  $S_h$ , the periodicity is consistent with our conjecture of  $\gamma_h$  (3.28) as a separating trajectory for  $P_{k,2}^0$  with  $\bar{H}(\gamma_h) = 0$  (see also Proposition 3.7). Again,  $\bar{H}$ , as approximated by (3.35), is constant along trajectories, in this case close to zero, up to high precision depending on  $h$ , as opposed to  $H$  which shows relatively large fluctuations. Additionally, we see in Figure 5 (c) that for large  $h$  the periodicity close to  $\gamma_{c,2}$  becomes less regular.

The conjecture that  $\bar{H}(\gamma_h) = 0$ , in case  $\bar{H}$  exists, is additionally supported in Figure 6, which shows the trajectory  $\gamma_h$  and the corresponding values of  $H + h^2 e^{-2y} \bar{H}_2$  (see (3.35)), which are of order  $10^{-10}$ . Furthermore, we consider trajectories for an initial point  $(x_{2,0}, y_{2,0})$  with  $x_{2,0} = 0$  and  $y_{2,0} < -\frac{1}{2} - \frac{h^2}{8}$ . Recall that in the time-continuous case these trajectories are unbounded solutions of the rescaled ODE (2.16). Indeed, we can track such unbounded solutions also with the Kahan method, as illustrated in Figure 7. As before, the figures in the first row show the trajectories (blue line) below  $S_h$  (red dashed line) while the figures in the second row show the corresponding values of  $\bar{H}$  as approximated in (3.35) (blue line) compared to the values of  $H$  (red dashed line), along the trajectories. We show these trajectories up to a number of iterations  $N$ , concatenating the forward and backward orbits, i.e. displaying  $(x_{2,-N}, y_{2,-N}), (x_{2,-N+1}, y_{2,-N+1}), \dots, (x_{2,N-1}, y_{2,N-1}), (x_{2,N}, y_{2,N})$ . We have chosen  $N$  such that at iteration  $N + 1$  (and  $-(N + 1)$ , respectively), the denominator  $(1 - hx + h^2/4)$  in the Kahan

map  $P_{2,k}^0$  (3.25) is close to changing sign or has just changed sign. This is the point where the Kahan discretization jumps away from the continuous-time solutions. This is indicated by a significant variation in  $H$  at time  $N$  and then followed by a significant change of  $\bar{H}$  at  $N + 1$ .

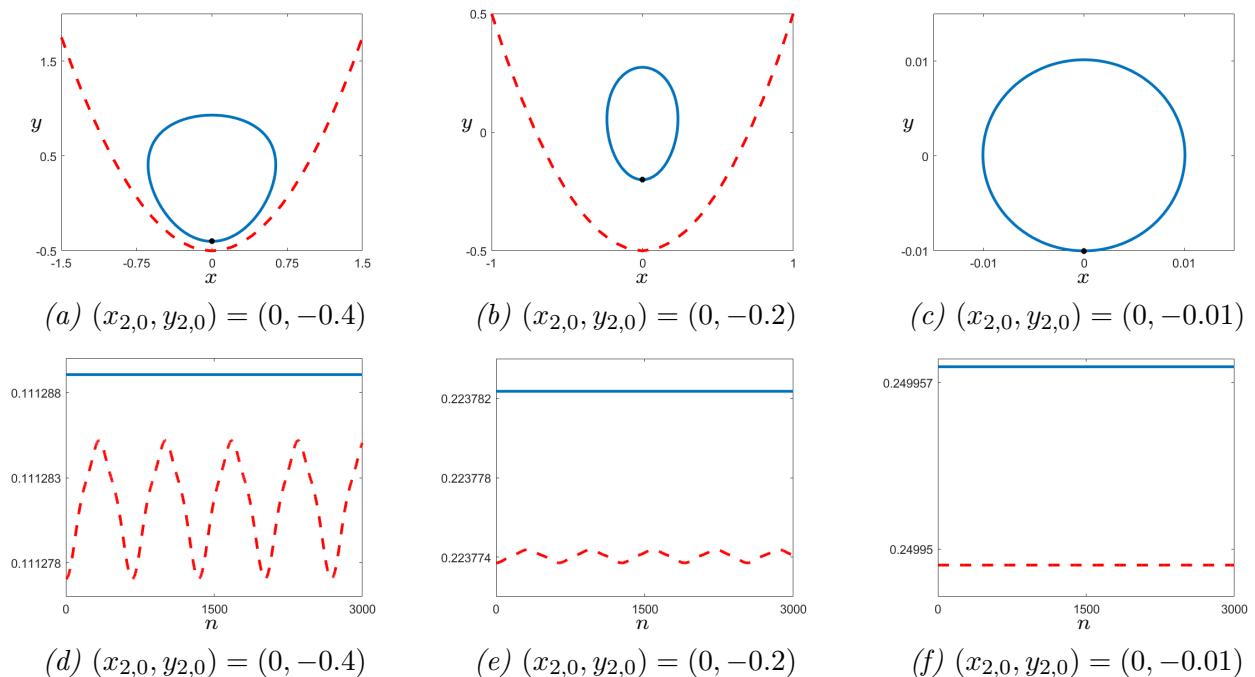


Figure 4: Figures (a)-(c) show trajectories for the Kahan map  $P^0$  in chart  $K_2$  (3.25) for different initial points  $(x_{2,0}, y_{2,0})$  (black dot) above the graph  $S_h$  (red dashed line), setting  $h = 0.01$ . Figures (d) -(f) show the corresponding values of  $\bar{H}(x_{2,n}, y_{2,n})$  in dependence of  $n$  as approximated in (3.35) (blue line) compared to the values of  $H$  (red dashed line) as given in (2.17).

The findings suggest that, if a conserved quantity  $\bar{H}$  exists, the special trajectory  $\gamma_h$  is a separatrix on compact sets, whose diameters depend on  $h$ , between periodic solutions ( $\bar{H} > 0$ ) and non-periodic, unbounded for  $h \rightarrow 0$ , solutions ( $\bar{H} < 0$ ), analogously to the ODE case. In addition, we note that, even if a conserved quantity  $\bar{H}$  does not exist, the dynamics of the Kahan discretization map  $P^0$  can be structured similarly to the ODE (2.16) around a special trajectory which separates different kinds of solutions preserving, presumably, the  $n$ -th partial sum of the formal series (3.32) up to order  $\mathcal{O}(h^{2(n+1)})$ .

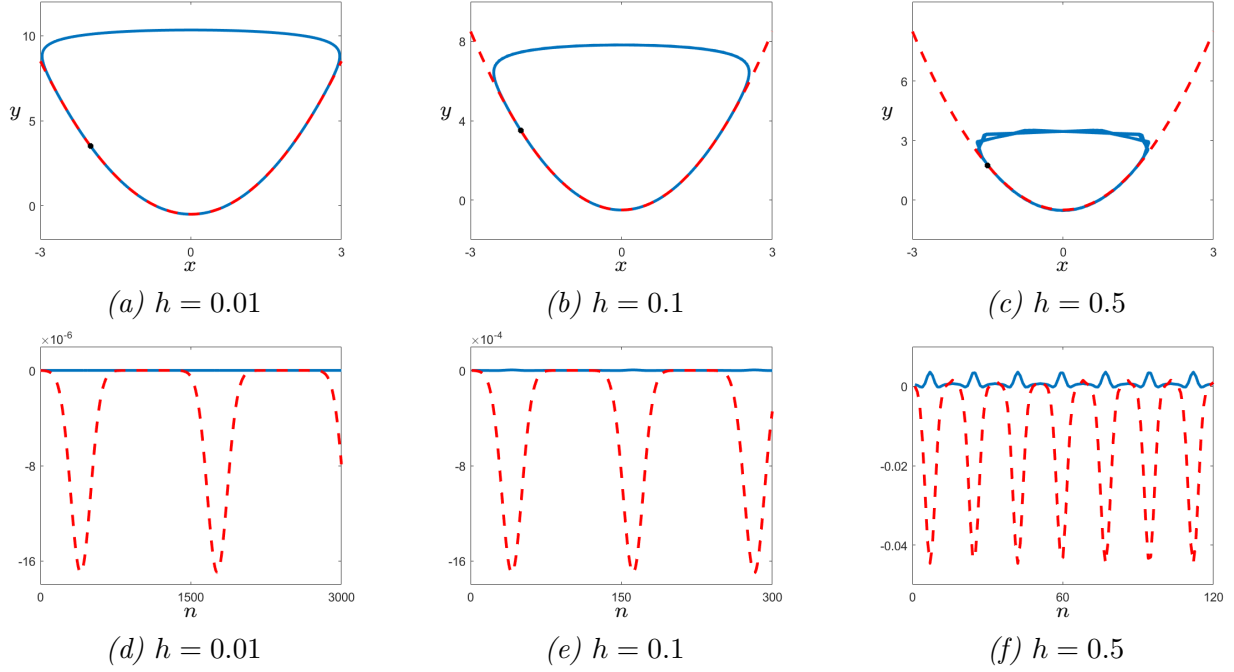


Figure 5: Figures (a)-(c) show trajectories for the Kahan map  $P^0$  in chart  $K_2$  (3.25) for different values of  $h$ , starting at an initial point  $(x_{2,0}, y_{2,0})$  (black dot) on the special ODE solution  $\gamma_{c,2}$  (red dashed line). Figures (d) - (f) show the corresponding values of  $\bar{H}(x_{2,n}, y_{2,n})$  in dependence of  $n$  as approximated in (3.35) (blue line) compared to the values of  $H$  (red dashed line) as given in (2.17).

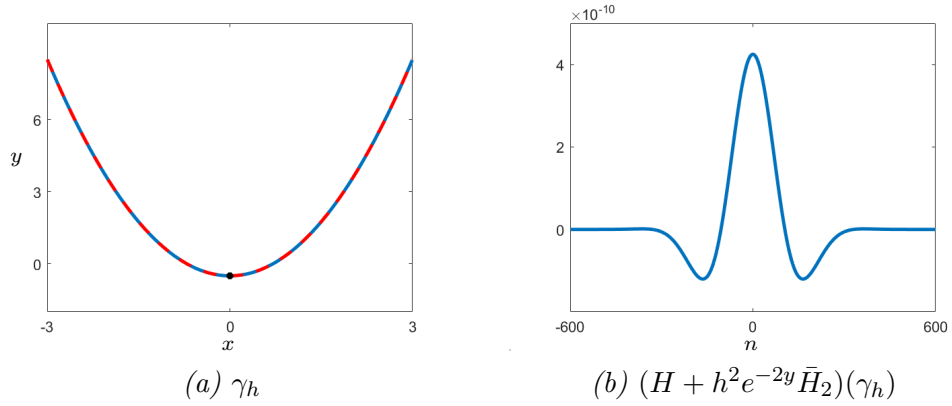


Figure 6: The trajectory  $\gamma_h$  (blue line) on  $S_h$  (red dashed line) with initial point  $(0, -1/2 - h^2/8)$  (black dot) for  $h = 0.01$  (Figure (a)) and the corresponding values of  $(H + h^2 e^{-2y} \bar{H}_2)(\gamma_h)$  with  $\bar{h}$  as in (3.34) (Figure (b)).

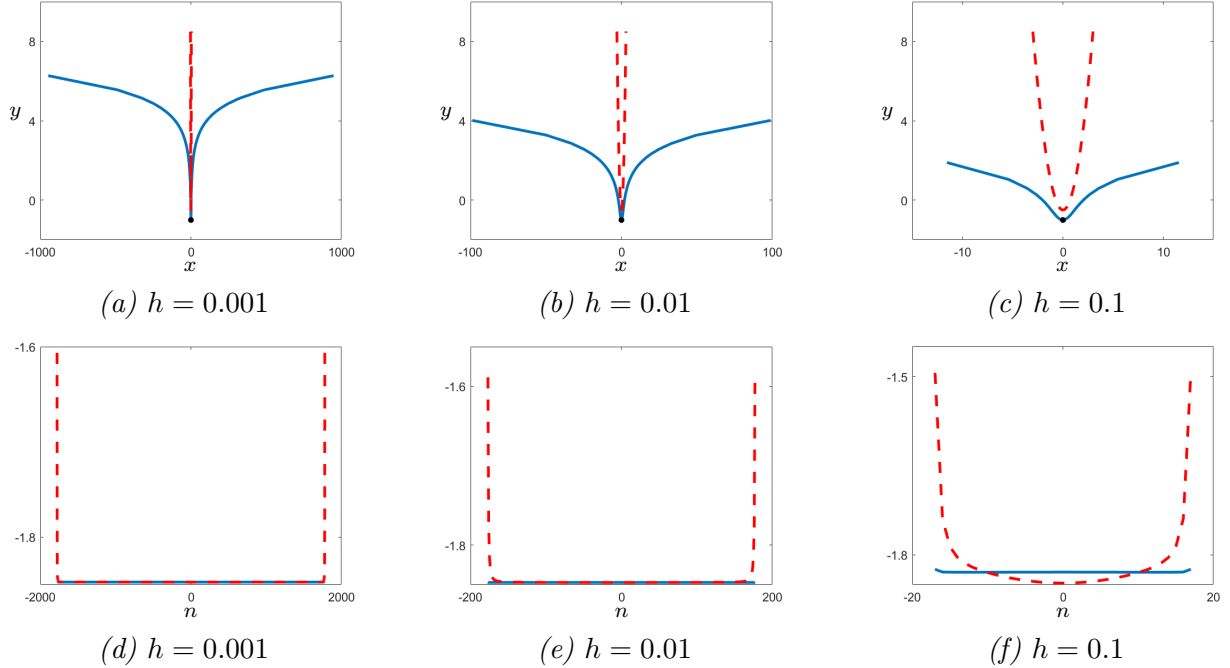


Figure 7: Figures (a)-(c) show trajectories  $(x_{2,-N}, y_{2,-N}), \dots, (x_{2,N}, y_{2,N})$  of the Kahan map  $P^0$  (3.25) in chart  $K_2$  for different values of  $h$  and the initial point  $(0, -1)$  (black dot) below  $S_h$  (red dashed line). The number  $N$  is chosen such that at  $N+1$  (and  $-(N+1)$  respectively) the denominator  $(1-hx+h^2/4)$  in  $P^0$  is changing sign. Figures (d)-(f) show the corresponding values of  $\bar{H}(x_{2,n}, y_{2,n})$  in dependence of  $n$  as approximated in (3.35) (blue line) compared to the values of  $H$  (red dashed line) as given in (2.17).

### 3.3.3 Symplectic discretization for Hamiltonian system

One strategy for making use of a conserved quantity in the time-discretized system concerns the potential coordinate transformation  $(x, y) \rightarrow (v, w)$  into a Hamiltonian system with Hamiltonian function  $\hat{H}$  which is then discretized by a symplectic method of order  $p$ . In this case, [11, Chapter IX, Theorem 8.1] implies the existence of a *modified Hamiltonian*  $\bar{H}$  such that on compact sets  $K$  we have

$$\begin{aligned} \bar{H}(v_n, w_n) &= \bar{H}(v_0, w_0) + \mathcal{O}(e^{-C/h}), & \hat{H}(v_n, w_n) &= \bar{H}(v_n, w_n) + \mathcal{O}(h^p), \\ \hat{H}(v_n, w_n) &= \hat{H}(v_0, w_0) + \mathcal{O}(h^p) \end{aligned} \quad (3.38)$$

over exponentially long time intervals  $nh \leq e^{C/h}$  for some constant  $C > 0$ .

In Appendix (A.1), we show how system (2.16) can be transformed into the ODE (A.1) with Hamiltonian  $\hat{H}$  (A.3) by using the invariant density  $1/\varphi$ . We observe immediately that the Kahan map  $P^0$  is not symplectic in the new coordinates since the invariant density  $1/\varphi_h$  of the map is not proportional to the invariant density  $1/\varphi$  of the corresponding ODE. Hence, this strategy does not seem to be applicable for the Kahan discretization.

Of course, one could deploy a symplectic method for discretizing the Hamiltonian system (A.1) and then transform back to the original coordinates, including the estimates from (3.38). The simplest such method, of order 1, is the symplectic Euler discretization which, for step size  $h > 0$ ,



reads (cf. [11, Chapter VI, Theorem 3.3])

$$\begin{aligned} v_{n+1} &= v_n - h \frac{\partial \hat{H}}{\partial w}(v_{n+1}, w_n), \\ w_{n+1} &= w_n + h \frac{\partial \hat{H}}{\partial v}(v_{n+1}, w_n). \end{aligned}$$

In the case of (A.1), the scheme can be written explicitly in terms of the map

$$\begin{aligned} v_{n+1} &= \frac{v_n - h e^{2w_n} + \frac{h}{4} + \frac{3h}{4} e^{w_n}}{1 - 2h e^{w_n}}, \\ w_{n+1} &= \frac{4v_n h + h(2+h) + w_n + e^{w_n}(h^2 + 2w_n h 2h)}{1 - 2h e^{w_n}}. \end{aligned}$$

However, transforming this map back into original coordinates via  $\rho^{-1}$  (A.2) gives extremely long formulas which are not identifiable as a particular discretization scheme. Hence, we refrain from following the strategy of using the transformation into Hamiltonian coordinates and applying a symplectic discretization scheme. Similarly, transforming the Kahan map via its invariant density  $1/\varphi_h$  into a symplectic map in the corresponding coordinates does not give workable formulas, aside from the fact that we would have no reference point for finding a conserved quantity of this symplectic map. In view of the transcendental formula involving an exponential function for the original Hamiltonian in the continuous-time case, it is also logical that we have not obtained nice closed analytical expressions using a discretization scheme that leads to a birational map.

Before we turn to a different approach, which will give the main result for the Kahan discretization of the folded canard problem in Section 3.3.4, we discuss briefly how a first integral for the discrete-time system or at least a quantity preserved up to an exponentially small error as in (3.38) could be applied for proving a discrete-time version of Theorem 2.1.

Assume for the following the existence of a quantity  $\bar{H}$  preserved by  $P^0$  (3.25) such that  $\bar{H}(\gamma_h(n), h) = 0$  for all  $|n| \leq M$  for some  $M \in \mathbb{N}$  depending on  $h$  (see also Proposition 3.7). We will see, in particular, that a situation as in (3.38) would be enough for the estimates we will need in the end. However, in the situation of transforming into Hamiltonian coordinates as described in Appendix A.1, the singularity of the invariant density  $1/\varphi$  at the parabola coinciding with the special solution  $\gamma_{c,2}$  would cause difficulties. This is another reason why we refrain from using a symplectic scheme in the new coordinates and a corresponding backward transformation for conducting a discrete Melnikov computation.

Recall from (3.23) that we can write the Kahan discretization in chart  $K_2$  as

$$\begin{pmatrix} \tilde{x} \\ \tilde{y} \end{pmatrix} = P^0(x, y, h) + r \begin{pmatrix} \hat{G}_1(x, y, h) \\ \hat{G}_2(x, y, h) \end{pmatrix} + \lambda \begin{pmatrix} \hat{J}_1(x, h) \\ \hat{J}_2(x, h) \end{pmatrix} + \mathcal{O}(r(\lambda + r)), \quad (3.39)$$

where  $P^0$  is the map in (3.25). Recall from Proposition 3.3 the center-stable manifold  $M_{a,2} = \kappa_{12}(M_{a,1})$  and center-unstable manifold  $M_{r,2} = \kappa_{12}(M_{r,1})$ . Let  $\gamma_h^a(n) = (x_{2,n}^a, y_{2,n}^a)$  and  $\gamma_h^r(n) = (x_{2,n}^r, y_{2,n}^r)$  be trajectories in  $M_{a,2}$  and  $M_{r,2}$  respectively where  $x_{2,0}^a = x_{2,0}^r = 0$ . Measuring the separation between  $M_{a,2}$  and  $M_{r,2}$  amounts to measuring  $y_{2,0}^a - y_{2,0}^r$ . In case such a quantity  $\bar{H}$  exists, this is equivalent to approximating the distance function

$$D(r, \lambda) := \bar{H}((0, y_{2,0}^a), h) - \bar{H}((0, y_{2,0}^r), h).$$

Similarly to [3, Proposition 2.1], we prove in Appendix A.3, Proposition A.1, the following first order approximation of  $D(r, \lambda)$ :

$$D(r, \lambda) = rd_r + \lambda d_\lambda + \mathcal{O}(|r| + |\lambda|)^2,$$

where

$$d_r := \sum_{n=1-M}^M \text{grad}_{x,y} \bar{H}(\gamma_h(n), h) \cdot \hat{G}(\gamma_h(n-1), h),$$

$$d_\lambda := \sum_{n=1-M}^M \text{grad}_{x,y} \bar{H}(\gamma_h(n)) \cdot \hat{J}(\gamma_h(n-1), h).$$

If we can show that  $d_\lambda \neq 0$  (A.11), the implicit function theorem can be used to deduce that  $D(r, \lambda^h(r)) = 0$  along a smooth function  $\lambda^h(r)$ . Hence, it would be enough to have a quantity  $\bar{H}$  which stays sufficiently close to  $H$  (2.17) and use the fact that  $\gamma_{c,2}(nh) = \gamma_h(n) + \mathcal{O}(h^2)$  in order to deduce  $d_\lambda \neq 0$  for sufficiently small  $h$ . In fact, taking  $H$  instead of  $\bar{H}$  in Proposition A.1 and thereby in formulas (A.11) and (A.12) with additional error estimates could lead to the required existence result for  $\lambda^h(r)$ . However, we prefer to conduct a different kind of Melnikov computation in the following which will be more insightful concerning the discrete-time dynamics of the Kahan map.

### 3.3.4 Melnikov computation along the invariant curve

Fortunately, we do not necessarily depend on the existence of a conserved quantity in the rescaled time discretization of system (2.11) in order to find a critical  $\lambda_c(\varepsilon)$ , for which canards are preserved. For the map (3.23), we can consider a different type of Melnikov computation, which we firstly derive in a more abstract setting as the discrete analogue of continuous-time results in [16] and, for a more general framework, [28].

Consider an invertible map

$$\begin{aligned} \tilde{x} &= F_1(x, y) + \mu G_1(x, y, \mu), \\ \tilde{y} &= F_2(x, y) + \mu G_2(x, y, \mu), \\ \tilde{\mu} &= \mu, \end{aligned} \tag{3.40}$$

where  $(x, y) \in \mathbb{R}^2$ ,  $\mu$  is a real parameter and  $F = (F_1, F_2)^\top$  and  $G = (G_1, G_2)^\top$  are some  $C^k$ ,  $k \geq 1$ , vector-valued maps. Analogously to [28], we can also write the following for  $\mu \in \mathbb{R}^m$ , as we will see later, but for reasons of clarity we restrict to  $\mu \in \mathbb{R}$ .

We assume that there exists a solution  $(\gamma(n), 0)$  to the dynamical system induced by (3.40), such that  $\gamma(n)$  and  $G(\gamma(n), 0)$  are of at most algebraic growth when  $n \rightarrow \pm\infty$ . Note that the linearization of (3.40) along  $(\gamma(n), 0)$  is given by

$$\tilde{w} = \begin{pmatrix} DF(\gamma(n)) & G(\gamma(n), 0) \\ 0 & 0 & 1 \end{pmatrix} w. \tag{3.41}$$

Furthermore, we formulate the following assumptions:

- (A1) There exist  $C^k$  smooth invariant manifolds  $M_\pm$ , parametrized by some  $C^k$  function  $y = g(x, \mu)$  and intersecting at  $\mu = 0$  along the smooth curve  $(\hat{\gamma}(t))_{t \in \mathbb{R}}$  with  $\{\hat{\gamma}(t) : t \in \mathbb{R}\} = \{(x, y) \in \mathbb{R}^2 : y = g(x, 0)\}$  and  $\hat{\gamma}(n) = \gamma(n)$  for all  $n \in \mathbb{Z}$ .

(A2) There exist solutions  $(w_{\pm}(n), 1)$  for (3.41), defined on  $\mathbb{Z}_{\geq 0}$  and  $\mathbb{Z}_{\leq 0}$  respectively, such that

$$T_{\gamma(n)}M_{\pm} = \text{span}\{(\hat{\gamma}'(n), 0), (w_{\pm}(n), 1)\}, \quad n \in \mathbb{Z}_0^{\pm},$$

and  $w_{\pm}$  are of at most algebraic growth when  $n \rightarrow \pm\infty$  respectively.

(A3) The dynamical system defined by the iterations of the *adjoint map*

$$\tilde{v} = \left(\mathbf{D}F(\gamma(n))^{\top}\right)^{-1} v \quad (3.42)$$

has a trajectory  $\psi(n)$  for  $n \in \mathbb{Z}$  with exponential decay at  $\pm\infty$ .

Note that for any solution  $\psi$  of (3.42) we have  $\langle\psi(0), \hat{\gamma}'(0)\rangle = 0$  and take  $\|\psi(0)\| = 1$ . Defining

$$\Sigma = \{(x, y, \mu) : \langle(x, y), \hat{\gamma}'(0)\rangle = 0\},$$

we can write the sets  $M_{\pm} \cap \Sigma$  in the form  $(\Delta_{\pm}(\mu)\psi(0), \mu)$  where  $\Delta_{\pm}$  are  $C^k$  smooth functions.

We can now show the following discrete time analogue to [16, Proposition 3.1]. The statement is similar to [9, Proposition 2.1] but we prefer this particular form in order to use computations for the continuous-time situation as an approximation in our arguments later.

**Proposition 3.8.** *Let  $\psi(n)$  be a solution to (3.42) with  $\|\psi(0)\| = 1$  and  $(w_{\pm}(n), 1)$  be the solutions of (3.41), defined on  $\mathbb{Z}_{\geq 0}$  and  $\mathbb{Z}_{\leq 0}$  respectively, with  $w_{\pm}(0) = \frac{d}{d\mu}\Delta_{\pm}(0)\psi(0)$ . Then we obtain the following measures of the separation between  $M_+$  and  $M_-$  at the section  $\Sigma$ .*

1. For every  $N \geq 1$ , we have

$$\begin{aligned} d_{\mu} &:= \frac{d}{d\mu}(\Delta_- - \Delta_+)(0) \\ &= \sum_{n=-N}^{N-1} \langle\psi(n+1), G(\gamma(n), 0)\rangle + \langle\psi(-N), w_-(-N)\rangle - \langle\psi(N), w_+(N)\rangle. \end{aligned} \quad (3.43)$$

2. Using assumptions (A1)-(A3), we obtain the well-defined formula

$$d_{\mu} = \sum_{n=-\infty}^{\infty} \langle\psi(n+1), G(\gamma(n), 0)\rangle. \quad (3.44)$$

*Proof.* Recall from equations (3.41) and (3.42) that

$$\begin{aligned} \psi(n+1) &= \left(\mathbf{D}F(\gamma(n))^{\top}\right)^{-1} \psi(n) \quad \text{for all } n \in \mathbb{Z}, \\ w_+(n+1) &= \mathbf{D}F(\gamma(n))w_+(n) + G(\gamma(n), 0) \quad \text{for all } n \in \mathbb{Z}_0^+, \\ w_-(n+1) &= \mathbf{D}F(\gamma(n))w_-(n) + G(\gamma(n), 0) \quad \text{for all } n \in \mathbb{Z}^-. \end{aligned}$$

Using these equations, we observe for all  $n \in \mathbb{Z}$  that

$$\begin{aligned} &\langle\psi(n+1), w_{\pm}(n+1)\rangle - \langle\psi(n), w_{\pm}(n)\rangle \\ &= \left\langle \left(\mathbf{D}F(\gamma(n))^{-1}\right)^{\top} \psi(n), \mathbf{D}F(\gamma(n))w_{\pm}(n) + G(\gamma(n), 0) \right\rangle - \langle\psi(n), w_{\pm}(n)\rangle \\ &= \langle\psi(n+1), G(\gamma(n), 0)\rangle. \end{aligned}$$

Hence, we can write for all  $N \geq 1$

$$\frac{d}{d\mu} \Delta_-(0) = \langle \psi(0), w_-(0) \rangle = \sum_{n=-N}^{-1} \langle \psi(n+1), G(\gamma(n), 0) \rangle + \langle \psi(-N), w_-(-N) \rangle,$$

and

$$\frac{d}{d\mu} \Delta_+(0) = \langle \psi(0), w_+(0) \rangle = - \sum_{n=0}^{N-1} \langle \psi(n+1), G(\gamma(n), 0) \rangle + \langle \psi(N), w_+(N) \rangle.$$

From here we obtain immediately formula (3.43).

In addition, we can deduce from the assumptions on  $G(\gamma(n), 0)$ ,  $w_{\pm}$  and  $\psi$  that letting  $N \rightarrow \infty$  leads to formula (3.44).  $\square$

We can use these considerations for showing the continuation of the canard connection for a change of  $\lambda$  depending on the change of the time separation parameter  $\varepsilon$ , by application of Proposition 3.8 to the situation of the Kahan map (3.23) in the rescaling chart  $K_2$ .

**Proposition 3.9.** *Consider system (3.23) in the form (3.40) with  $\lambda = \mu$  (for  $r = 0$ ) or  $r = \mu$  (for  $\lambda = 0$ ) respectively. Then the separation between the center-stable manifold  $\hat{M}_{a,2} = \kappa_{12}(\hat{M}_{a,1})$  and center-unstable manifold  $\hat{M}_{r,2} = \kappa_{12}(\hat{M}_{r,1})$ , which intersect along  $\gamma_h$  (3.28), satisfies formula (3.43) in Proposition 3.8.*

*Additionally, if  $\psi$  satisfies exponential decay as in Assumption 3, we also have formula (3.44).*

*Proof.* Assumption 1 and 2 are clear due to the definition of  $\hat{M}_{a,2}$  and  $\hat{M}_{r,2}$  as center manifolds and the fact that  $\kappa_{12}$  is algebraic. Hence, the claim follows immediately.  $\square$

Since the splitting of the manifolds  $\hat{M}_{a,2}$  and  $\hat{M}_{r,2}$  depends on the two parameters  $(r, \lambda)$ , we can define the distance function as

$$D(r, \lambda) := \Delta_-^2(r, \lambda) - \Delta_+^2(r, \lambda),$$

where  $\Delta_{\pm}^2(r, \lambda)$  are the two-dimensional extensions to  $\Delta_{\pm}$  (see [28] for continuous time) such that  $\Delta_{\pm}^2(0, \lambda) = \Delta_{\pm}(\lambda)$  and  $\Delta_{\pm}^2(r, 0) = \Delta_{\pm}(r)$  respectively. With Proposition 3.9, we obtain the first order expansion

$$D(r, \lambda) = d_{\lambda} \lambda + d_r r + \mathcal{O}(2), \quad (3.45)$$

where  $\mathcal{O}(2)$  denotes higher order terms.

We are now prepared to show our main result.

**Theorem 3.10.** *Consider the forward and backward iterations of the Kahan discretization map  $P_K$  for system (3.12). Then there exist  $\varepsilon_0, h_0 > 0$  and a smooth function  $\lambda_c^h(\sqrt{\varepsilon})$  defined on  $[0, \varepsilon_0]$  such that for  $\varepsilon \in [0, \varepsilon_0]$  and  $h \in (0, h_0]$  the following holds:*

1. *The attracting slow manifold  $S_{a,\varepsilon,h}$  and the repelling slow manifold  $S_{r,\varepsilon,h}$  intersect, i.e. exhibit a maximal canard, if and only if  $\lambda = \lambda_c^h(\sqrt{\varepsilon})$ .*
2. *For any  $\delta > 0$ , the function  $\lambda_c^h$  has the expansion*

$$\lambda_c^h(\sqrt{\varepsilon}) = -C\varepsilon + \mathcal{O}(\varepsilon),$$

*where  $C$  is given as in (2.10).*

*Proof.* Firstly, we will work in chart  $K_2$  and approximate  $d_\lambda$  and  $d_r$  in (3.45). For that purpose, we observe from (3.29) that, for fixed  $h$ , the Jacobian of  $P^0$  (3.25) is given by

$$D_{x,y}P^0(x,y,h) = \begin{pmatrix} 1 + 2xh & -h \\ h & 1 \end{pmatrix} + \mathcal{O}(h^2).$$

This shows that the approximation of the corresponding variational equation of the ODE (2.16) with Jacobian

$$Df = \begin{pmatrix} 2x & -1 \\ 1 & 0 \end{pmatrix}$$

is of at least the same order as an Euler approximation. Furthermore, we obtain for the adjoint problem (3.42) along  $\gamma_h$  that

$$\tilde{\psi}_h = \begin{pmatrix} 1 - (nh)h & -h \\ h & 1 \end{pmatrix} \psi_h + \mathcal{O}(h^2). \quad (3.46)$$

We know from [28] that the linear adjoint equation for system (2.16) along  $\gamma_{c,2}$  (2.18) reads

$$\psi' = -Df(\gamma_{c,2}(t_2))^\top \psi = \begin{pmatrix} -t_2 & -1 \\ 1 & 0 \end{pmatrix} \psi, \quad (3.47)$$

where the only solution decaying exponentially in forward and backward time is given as

$$\psi(t) = \begin{pmatrix} -t_2 e^{-t_2^2/2} \\ e^{-t_2^2/2} \end{pmatrix}.$$

Hence, comparing (3.46) with (3.47), we deduce that

$$\psi(nh) = \psi_h(n) + \mathcal{O}(h)$$

on compact time intervals. Moreover, by noting that  $\gamma_{c,2}^1(nh) = \gamma_h^1(n)$  for the first and  $\gamma_{c,2}^2(nh) = \gamma_h^2(n) + \mathcal{O}(h^2)$  for the second vector component, and by using that the Kahan discretization is a second order method, we have that

$$hJ(\gamma(nh)) = \hat{J}(\gamma_h(n), h) + \mathcal{O}(h^2), \quad hG(\gamma(nh)) = \hat{G}(\gamma_h(n), h) + \mathcal{O}(h^2),$$

where  $\hat{J}, \hat{G}$  are as in (3.23), and  $J = (J_1, J_2)^\top = (0, -1)^\top$  and  $G = (G_1, G_2)^\top$  as in (2.15). Using these estimates, we obtain, similarly to before, that

$$w_\pm = w_\pm^h + \mathcal{O}(h),$$

where  $w_\pm^h$  denote the algebraically growing solutions of the variational equations for discrete time (see Propositions 3.8 and 3.9) and  $w_\pm$  for continuous time (see [28]). Further recall that the Melnikov integrals along  $\gamma_{c,2}$  can be solved explicitly, yielding

$$\begin{aligned} \int_{-\infty}^{\infty} \langle \psi(t), J(\gamma_{c,2}(t)) \rangle dt &= - \int_{-\infty}^{\infty} e^{-t^2/2} dt = -\sqrt{2\pi}, \\ \int_{-\infty}^{\infty} \langle \psi(t), G(\gamma_{c,2}(t)) \rangle dt &= \frac{1}{8} \int_{-\infty}^{\infty} (-4a_5 - (4a_1 + 2a_2 - 2a_4 - 2a_5)t^2 + (a_2 - a_3)t^4) e^{-t^2/2} dt \\ &= -C\sqrt{2\pi}, \end{aligned}$$

where  $a_i$  and  $C$  are as introduced in Section 2.2.

Let now  $\delta > 0$  be arbitrarily small. Then there is an  $N \in \mathbb{N}$  such that for  $T := Nh$  we have

$$2 \int_T^\infty e^{-t^2/2} dt + e^{-T^2/2} T (\|w_-(T)\| + \|w_+(T)\|) < \delta.$$

Combining this with formula (3.43) and the estimates from above, we obtain

$$\begin{aligned} |-\sqrt{2\pi} - d_\lambda| &= \left| \int_{-\infty}^\infty \langle \psi(t), J(\gamma_{c,2}(t)) \rangle dt - \right. \\ &\quad \left. \sum_{n=-N}^{N-1} \langle \psi_h(n+1), \hat{J}(\gamma_h(n), h) \rangle - \langle \psi_h(-N), w_-^h(-N) \rangle + \langle \psi_h(N), w_+^h(N) \rangle \right| \\ &\leq 2 \int_T^\infty e^{-t^2/2} dt + \left| \int_{-T}^T \langle \psi(t), J(\gamma_{c,2}(t)) \rangle dt - \sum_{n=-N}^{N-1} \langle \psi_h(n+1), \hat{J}(\gamma_h(n), h) \rangle \right| \\ &\quad + e^{-T^2/2} T (\|w_-(T)\| + \|w_+(T)\|) + K_1(\delta)h \\ &< \delta + (K_2(\delta) + K_1(\delta))h, \end{aligned}$$

where  $K_1(\delta), K_2(\delta) > 0$  are constants only depending on  $T$  and thereby on  $\delta$ . In other words, we have that

$$|-\sqrt{2\pi} - d_\lambda| = \mathcal{O}(\delta) + \mathcal{O}(h). \quad (3.48)$$

Similarly, we obtain

$$|-C\sqrt{2\pi} - d_r| = \mathcal{O}(\delta) + \mathcal{O}(h).$$

Recall from (3.45) that

$$D(r, \lambda) = d_\lambda \lambda + d_r r + \mathcal{O}(2),$$

where  $D(0, 0) = 0$ . Hence, we can deduce from (3.48) with the Implicit Function Theorem that, for  $h$  sufficiently small, there is a smooth function  $\lambda^h(r)$  such that

$$D(r, \lambda^h(r)) = 0$$

in a small neighbourhood of  $(0, 0)$ . Transforming back from  $K_2$  into original coordinates proves the first claim.

Furthermore, we obtain

$$\lambda^h(r) = -\frac{d_r}{d_\lambda} r + \mathcal{O}(2) = -Cr + \mathcal{O}(r\delta) + \mathcal{O}(rh).$$

Transformation into original coordinates gives

$$\lambda_c^h(\sqrt{\varepsilon}) = -C\varepsilon + \mathcal{O}(\varepsilon\delta) + \mathcal{O}(\varepsilon^{3/2}h).$$

Hence, the second claim follows.  $\square$

Numerical computations show that  $h_0$  in Theorem 3.10 does not have to be extremely small but that our results are quite robust for different step sizes. In Figure 8, we display such computations for the case  $a_1 = 1, a_2 = a_4 = a_5 = 0$ . In this case, the rescaled Kahan discretization in chart  $K_2$  is given by

$$\begin{aligned} \tilde{x} &= \frac{x - hy + \frac{h}{2}xr - \frac{h^2}{4}x + \frac{h^2}{2}\lambda}{1 - hx - \frac{h}{2}r + \frac{h^2}{4}}, \\ \tilde{y} &= \frac{y - hxy - \frac{h}{2}yr - \frac{h^2}{2}x^2 - h\lambda + h^2x\lambda + hx + \frac{h^2}{2}\lambda r - \frac{h^2}{4}y}{1 - hx - \frac{h}{2}r + \frac{h^2}{4}}. \end{aligned} \quad (3.49)$$

Hence, we obtain

$$\hat{G}_1(x, y, h) = \frac{hx - \frac{h^2}{2}y - \frac{h^2}{2}x^2}{\left(1 - hx + \frac{h^2}{4}\right)^2}, \quad \hat{G}_2(x, y, h) = \frac{\frac{h^2}{2}x - \frac{h^3}{4}y - \frac{h^3}{4}x^2}{\left(1 - hx + \frac{h^2}{4}\right)^2}. \quad (3.50)$$

For different values of  $h$  and  $N$  we calculate

$$d_h^\lambda(N) := \sum_{n=-N}^{N-1} \langle \psi_h(n+1), \hat{J}(\gamma_h(n)) \rangle \approx d_\lambda,$$

and, for the situation of (3.49) with  $\hat{G}$  as in (3.50),

$$d_h^r(N) := \sum_{n=-N}^{N-1} \langle \psi_h(n+1), \hat{G}(\gamma_h(n), h) \rangle \approx d_r,$$

We compare these quantities with the values of the respective continuous-time integrals  $d_c^\lambda = -\sqrt{2\pi}$  and  $d_c^r = -\sqrt{2\pi}/2$  (we have  $C = 1/2$  in this case).

We observe in Figure 8 that the sums converge very fast for relatively small  $hN$  in both cases. Additionally, we see that  $|d_h^\lambda(N) - d_c^\lambda|$  is significantly smaller than  $|d_h^r(N) - d_c^r|$  for the same values of  $h$ . Note that the computations indicate that Theorem 3.10 holds for the chosen values of  $h$  since  $d_\lambda \approx -\sqrt{2\pi} + (d_h^\lambda(N) - d_c^\lambda)$  is clearly distant from 0.

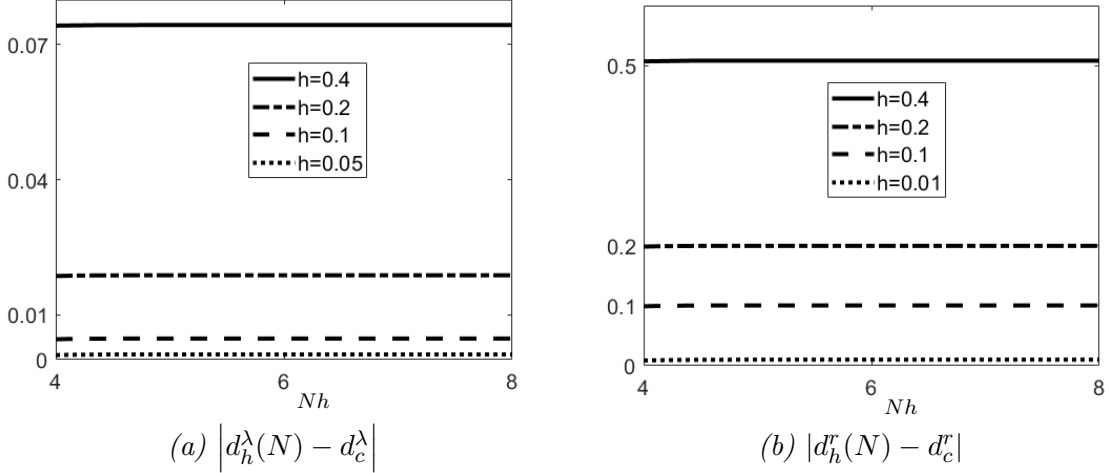


Figure 8: The integral errors (a)  $|d_h^\lambda(N) - d_c^\lambda|$  and (b)  $|d_h^r(N) - d_c^r|$  for different values of  $h$  and  $N \in \mathbb{N}$ .

## References

- [1] E. Benoît, J. Callot, F. Diener, and M. Diener. Chasse au canards. *Collect. Math.*, 31:37–119, 1981.
- [2] E. Celledoni, R. I. McLachlan, B. Owren, and G. R. W. Quispel. Geometric properties of Kahan’s method. *J. Phys. A*, 46(2):025201, 12, 2013.
- [3] A. Delshams and R. Ramírez-Ros. Poincaré-Melnikov-Arnold method for analytic planar maps. *Nonlinearity*, 9(1):1–26, 1996.
- [4] F. Dumortier. *Singularities of vector fields*, volume 32 of *Monografías de Matemática [Mathematical Monographs]*. Instituto de Matemática Pura e Aplicada, Rio de Janeiro, 1978.
- [5] F. Dumortier. Techniques in the theory of local bifurcations: blow-up, normal forms, nilpotent bifurcations, singular perturbations. In *Bifurcations and periodic orbits of vector fields (Montreal, PQ, 1992)*, volume 408 of *NATO Adv. Sci. Inst. Ser. C Math. Phys. Sci.*, pages 19–73. Kluwer Acad. Publ., Dordrecht, 1993.
- [6] F. Dumortier and R. Roussarie. Canard cycles and center manifolds. *Mem. Amer. Math. Soc.*, 121(577):x+100, 1996. With an appendix by Cheng Zhi Li.
- [7] M. Engel and C. Kuehn. Discretized fast-slow systems near transcritical singularities. *arXiv:1806.06561*, 2018.
- [8] N. Fenichel. Geometric singular perturbation theory for ordinary differential equations. *J. Differential Equations*, 31:53–98, 1979.
- [9] M. L. Glasser, V. G. Papageorgiou, and T. C. Bountis. Mel’nikov’s function for two-dimensional mappings. *SIAM J. Appl. Math.*, 49(3):692–703, 1989.
- [10] I. Gucwa and P. Szmolyan. Geometric singular perturbation analysis of an autocatalator model. *Discr. Cont. Dyn. Syst. S*, 2(4):783–806, 2009.
- [11] E. Hairer, C. Lubich, and G. Wanner. *Geometric numerical integration*, volume 31 of *Springer Series in Computational Mathematics*. Springer-Verlag, Berlin, second edition, 2006. Structure-preserving algorithms for ordinary differential equations.
- [12] M. W. Hirsch, C. C. Pugh, and M. Shub. *Invariant manifolds*. Lecture Notes in Mathematics, Vol. 583. Springer-Verlag, Berlin-New York, 1977.
- [13] C. K. R. T. Jones. Geometric singular perturbation theory. In *Dynamical systems (Montecatini Terme, 1994)*, volume 1609 of *Lecture Notes in Math.*, pages 44–118. Springer, Berlin, 1995.
- [14] W. Kahan. *Unconventional numerical methods for trajectory calculations*. Unpublished lecture notes, 1993.
- [15] M. Krupa and P. Szmolyan. Extending geometric singular perturbation theory to nonhyperbolic points—fold and canard points in two dimensions. *SIAM J. Math. Anal.*, 33(2):286–314, 2001.



- [16] M. Krupa and P. Szmolyan. Extending slow manifolds near transcritical and pitchfork singularities. *Nonlinearity*, 14(6):1473–1491, 2001.
- [17] M. Krupa and P. Szmolyan. Relaxation oscillation and canard explosion. *J. Differential Equations*, 174(2):312–368, 2001.
- [18] C. Kuehn. Normal hyperbolicity and unbounded critical manifolds. *Nonlinearity*, 27(6):1351–1366, 2014.
- [19] C. Kuehn. *Multiple time scale dynamics*, volume 191 of *Applied Mathematical Sciences*. Springer, Cham, 2015.
- [20] C. Kuehn. A remark on geometric desingularization of a non-hyperbolic point using hyperbolic space. *J. Phys. Conf. Ser.*, 727:012008, 2016.
- [21] M. E. L. Arcidiacono and C. Kuehn. Discretized fast-slow systems near pitchfork singularities. *arXiv:1902.06561*, 2019.
- [22] P. D. Maeschalck and F. Dumortier. Time analysis and entry-exit relation near planar turning points. *J. Difference Equ. Appl.*, 215:225–267, 2005.
- [23] P. D. Maeschalck and F. Dumortier. Singular perturbations and vanishing passage through a turning point. *J. Differential Equations*, 248:2294–2328, 2010.
- [24] P. D. Maeschalck and M. Wechselberger. Neural excitability and singular bifurcations. *J. Math. Neurosci.*, 5(1):16, 2015.
- [25] K. Nipp and D. Stoffer. *Invariant manifolds in discrete and continuous dynamical systems*, volume 21 of *EMS Tracts in Mathematics*. European Mathematical Society (EMS), Zürich, 2013.
- [26] M. Petrera and Y. Suris. New results on integrability of the kahan-hirota-kimura discretizations. *arXiv:1805.12490*, 2018.
- [27] A. M. Stuart and A. R. Humphries. *Dynamical systems and numerical analysis*, volume 2 of *Cambridge Monographs on Applied and Computational Mathematics*. Cambridge University Press, Cambridge, 1996.
- [28] M. Wechselberger. Extending Melnikov theory to invariant manifolds on non-compact domains. *Dyn. Syst.*, 17(3):215–233, 2002.
- [29] S. Wiggins. *Normally hyperbolic invariant manifolds in dynamical systems*, volume 105 of *Applied Mathematical Sciences*. Springer-Verlag, New York, 1994. With the assistance of György Haller and Igor Mezić.

# Appendix A

## A.1 Transformation to Hamiltonian coordinates

Recall from (2.17) that the rescaled ODE (2.16), without higher order terms in chart  $K_2$ , possesses the first integral

$$H(x, y) = \frac{1}{4}e^{-2y}(2y - 2x^2 + 1).$$

It is then easy to observe that system (2.16) has the invariant measure

$$\mu^\pm(dx, dy) = \frac{1}{\pm\varphi(x, y)}dx dy,$$

where

$$\varphi(x, y) = 2y - 2x^2 + 1,$$

on the Borel sets of

$$U^\pm = \{(x, y) \in \mathbb{R}^2 : \pm(2y - 2x^2 + 1) > 0\}$$

respectively, i.e. above and below the separating solution  $\gamma_{c,2}$ . In the following, we focus on  $\mu := \mu^+$  on  $U := U^+$ . The other case is analogous.

Note that the existence of an invariant density means that, via an appropriate coordinate transformation, system (2.16) generates an area-preserving, and thereby symplectic, flow. In more detail, we introduce the diffeomorphic coordinate transformation  $\rho(x, y) = (v, w)$  on  $U$ , given by

$$\begin{aligned} v &= \rho_1(x, y) = \frac{1}{2}x - x^2 + y, \\ w &= \rho_2(x, y) = \ln(-2x^2 + 2y + 1). \end{aligned}$$

Indeed, we have  $|\det(D\rho(x, y))| = 1$  such that the flow generated by the ODE

$$\begin{aligned} v' &= \frac{1}{4}(-4e^{2w} + 1 + e^w(8v + 3)), \\ w' &= 4v - 2e^w + 2 \end{aligned} \tag{A.1}$$

is area-preserving in  $\mathbb{R}^2$  and, hence, symplectic. By [11, Chapter VI, Theorem 2.6] we can deduce that the ODE (A.1) is *locally Hamiltonian*, i.e. for every point  $z \in U$  there exists a neighbourhood where (A.1) is Hamiltonian. In fact, we can find a global Hamiltonian function  $\hat{H}$  via  $\tilde{H} = (H \circ \rho^{-1})(v, w)$  where  $\rho^{-1} = (\rho_1^{-1}, \rho_2^{-1})$  is given by

$$\begin{aligned} x &= \rho_1^{-1}(v, w) = 2v - e^w + 1, \\ y &= \rho_2^{-1}(v, w) = -\frac{3}{2}e^w + \frac{1}{2} + 4v(1 + v - e^w) + e^{2w}. \end{aligned} \tag{A.2}$$

One can easily check that

$$\hat{H}(v, w) = -\frac{1}{4}\ln \tilde{H} = \frac{1 + \ln 4}{4} + \frac{e^{2w}}{2} + 2v - \frac{w}{4} + 2v^2 - \frac{1}{4}e^w(8v + 3) \tag{A.3}$$

is a Hamiltonian function for system (A.1).

## A.2 Derivation of a formal conserved quantity for Kahan discretization

Recall that for an ODE of the form (3.8) the Kahan discretization is characterized by the map  $\Lambda_f$  (3.10). Assume that (3.8) admits a smooth conserved quantity  $H : \mathbb{R}^n \rightarrow \mathbb{R}$ , which means that

$$\sum_{i=1}^n \frac{\partial H(z)}{\partial z_i} f_i(z) = 0. \quad (\text{A.4})$$

We observe that taking the Lie derivative of the left hand side of (A.4) yields

$$0 = \sum_{j=1}^n \frac{\partial}{\partial z_j} \left( \sum_{i=1}^n \frac{\partial H(z)}{\partial z_i} f_i(z) \right) f_j(z) = \sum_{i,j=1}^n \frac{\partial^2 H(z)}{\partial z_i \partial z_j} f_i(z) f_j(z) + \sum_{i,j=1}^n \frac{\partial H(z)}{\partial z_i} \frac{\partial f_i(z)}{\partial z_j} f_j(z). \quad (\text{A.5})$$

Using a twofold Taylor expansion of  $H(\Lambda_f(z, h))$  at  $h = 0$  and writing  $\tilde{z} = \Lambda_f(z, h)$ , we compute

$$\begin{aligned} H(\tilde{z}) &= H \left( z + hf(z) + \frac{h^2}{2} f(z) Df(z) + \mathcal{O}(h^3) \right) \\ &= H(z) + h \sum_{i=1}^n \frac{\partial H(z)}{\partial z_i} f_i(z) \\ &\quad + \frac{h^2}{2} \left( \sum_{i,j=1}^n \frac{\partial^2 H(z)}{\partial z_i \partial z_j} f_i(z) f_j(z) + \sum_{i,j=1}^n \frac{\partial H(z)}{\partial z_i} \frac{\partial f_i(z)}{\partial z_j} f_j(z) \right) + \mathcal{O}(h^3). \end{aligned}$$

Hence, we obtain with (A.4) and (A.5) that

$$H(\tilde{z}) = H(z) + \mathcal{O}(h^3),$$

and, due to the smoothness of the functions  $f$  and  $H$ , we can expand  $H(\tilde{z})$  in powers of  $h$  as

$$H(\tilde{z}) = H(z) + h^3 G_3(z) + h^4 G_4(z) + h^5 G_5(z) + \dots, \quad (\text{A.6})$$

for some smooth functions  $G_i$ ,  $i = 3, 4, 5, \dots$

Since the Kahan method is a symmetric linear discretization scheme, a conserved quantity for  $\Lambda_f$ , if it exists, must be an even function of the discretization parameter  $h$ . This suggests the following formal Ansatz for a conserved quantity  $\bar{H} : \mathbb{R}^n \times [0, h_0] \rightarrow \mathbb{R}$  for some  $h_0 > 0$ , i.e.  $\bar{H}$  satisfies  $\bar{H}(z, h) = \bar{H}(\tilde{z}, h)$  on  $\mathbb{R}^n \times [0, h_0]$ :

$$\bar{H}(z, h) = H(z) + h^2 H_2(z) + h^4 H_4(z) + h^6 H_6(z) + \dots, \quad (\text{A.7})$$

where the functions  $H_i$ ,  $i = 2, 4, 6, \dots$ , are to be determined. Given the existence of such a  $\bar{H}(z, h)$ , the function  $H_2$  can be identified by using the conservation property, the expansions (A.6) and (A.7) and a Taylor expansion of  $H_2(\Lambda_f(z, h))$  similar to  $H(\Lambda_f(z, h))$ :

$$\begin{aligned} H(z) + h^2 H_2(z) + \mathcal{O}(h^4) &= \bar{H}(z, h) = \bar{H}(\tilde{z}, h) = H(\tilde{z}) + h^2 H_2(\tilde{z}) + \mathcal{O}(h^4) \\ &= H(z) + h^2 H_2(z) + h^3 \left( G_3(z) + \frac{\partial H_2(z)}{\partial z_i} f_i(z) \right) + \mathcal{O}(h^4). \end{aligned}$$

Hence, we observe that  $H_2$  can be obtained by solving the differential equation

$$G_3(z) + \frac{\partial H_2(z)}{\partial z_i} f_i(z) = 0. \quad (\text{A.8})$$

The other functions  $H_4, H_6, \dots$  can then be determined in a similar manner.

### A.3 Poincare-Melnikov-Arnold methods for maps

Consider the map (3.39), with  $P^0$  as in (3.25). As described in Section 3.3.3, recall the center-stable manifold  $M_{a,2} = \kappa_{12}(M_{a,1})$  and center-unstable manifold  $M_{r,2} = \kappa_{12}(M_{r,1})$  with trajectories  $\gamma_h^a(n) = (x_{2,n}^a, y_{2,n}^a)$  and  $\gamma_h^r(n) = (x_{2,n}^r, y_{2,n}^r)$  respectively where  $x_{2,0}^a = x_{2,0}^r = 0$ . Assuming the existence of a conserved quantity  $\bar{H}$  for  $P^0$ , with  $\bar{H}(\gamma_h(n), h) = 0$  for all  $|n| \leq M$  for some  $M \in \mathbb{N}$  depending on  $h$ , we measure the separation between  $M_{a,2}$  and  $M_{r,2}$  via the distance function

$$D(r, \lambda) := \bar{H}((0, y_{2,0}^a), h) - \bar{H}((0, y_{2,0}^r), h).$$

Similarly to [3, Proposition 2.1], where homoclinic orbits are considered, we can give the following first order approximation of  $D(r, \lambda)$  under a specific decay assumptions on  $\bar{H}(\gamma_h^a(-n), h) - \bar{H}(\gamma_h^r(n), h)$ :

**Proposition A.1.** *Let  $h$  be small enough such that the orbits  $\gamma_h(n), \gamma_h^a(n), \gamma_h^r(n)$  satisfy the requirements above for all  $n \in \mathbb{Z}$  with  $|n| \leq M$  where  $M \in \mathbb{N}$  is such that*

$$\bar{H}(\gamma_h^a(-M), h) - \bar{H}(\gamma_h^r(M), h) = \mathcal{O}(|r| + |\lambda|^2). \quad (\text{A.9})$$

Then the distance function can be expanded as

$$D(r, \lambda) = rd_r + \lambda d_\lambda + \mathcal{O}(|r| + |\lambda|^2), \quad (\text{A.10})$$

where

$$d_r := \sum_{n=1-M}^M \text{grad}_{x,y} \bar{H}(\gamma_h(n), h) \cdot \hat{G}(\gamma_h(n-1), h), \quad (\text{A.11})$$

$$d_\lambda := \sum_{n=1-M}^M \text{grad}_{x,y} \bar{H}(\gamma_h(n)) \cdot \hat{J}(\gamma_h(n-1), h). \quad (\text{A.12})$$

*Proof.* Recall from our assumptions that  $D(0, 0) = 0$  and  $D$  is smooth. We show the expansion in  $r$ . The result for  $\lambda$  can be obtained analogously.

We assume  $\lambda = 0$  and observe that

$$D(r, 0) = \bar{H}(\gamma_h^a(-M), h) - \bar{H}(\gamma_h^r(M), h) + \sum_{n=1-M}^M \bar{H}(\gamma_h^\sigma(n), h) - \bar{H}(\gamma_h^\sigma(n-1), h),$$

where  $\sigma = a$  for  $n \leq 0$  and  $\sigma = r$  for  $n > 0$ . Writing  $P_K^r$  for the map corresponding with (3.23) restricted to  $(x, y, h)$ , we can deduce, by assumption (A.9) and the definition of  $\gamma_h^\sigma$ , that

$$D(r, 0) = \sum_{n=1-M}^M \left( \bar{H} \circ P_K^r - \bar{H} \right) (\gamma_h^\sigma(n-1), h) + \mathcal{O}(r^2).$$

Using (3.23) (or (3.39) respectively), we have that  $\gamma_h^\sigma(n-1) = \gamma_h(n-1) + \mathcal{O}(r)$  and the first order expansion

$$\bar{H} \circ P_K^r - \bar{H} = r(\text{grad}_{x,y} \bar{H} \circ P^0) \cdot \hat{G} + \mathcal{O}(r^2).$$

Hence, the claim follows.  $\square$

Note that it is not a priori clear why assumption (A.9) should be satisfied in this context. However, if one can show that  $\bar{H}$  and  $\gamma_h^a, \gamma_h^r$  are sufficiently close to their continuous-time counterparts – see e.g. (3.38) –, knowledge about the quantities in the ODE system, where this assumption is fulfilled, can be used.